RELATIONSHIP BETWEEN CORNEAL BIOMECHANICS AND LAMINA CRIBROSA SHAPE IN LOW AND HIGH MYOPES

XU FANGYU

MPhil

The Hong Kong Polytechnic University

2022

The Hong Kong Polytechnic University

School of Optometry

Relationship between Corneal Biomechanics and Lamina Cribrosa Shape in Low and High Myopes

Xu Fangyu

A thesis submitted in partial fulfillment of the requirements for the degree of Master of Philosophy

January 2022

CERTIFICATE OF ORIGINALITY

I hereby declare that this thesis is my own work and that, to the best of my knowledge and belief, it reproduces no material previously published or written, nor material that has been accepted for the award of any other degree or diploma, except where due acknowledgement has been made in the text.

XU Fangyu

Abstract

Thesis title: **Relationship between corneal biomechanics and lamina cribrosa shape in low and high myopes**

Chief supervisor: **Dr. Kwok Cheung Andrew LAM**

High myopia is an important risk factor for open-angle glaucoma that is possibly caused by weakened ocular biomechanics. The cornea and lamina cribrosa both develop from mesoderm with a similar extracellular matrix and they might share similar tissue biomechanics. The lamina cribrosa is recognized as the site of glaucomatous damage, but its biomechanical properties are difficult to measure. Several research groups have used optical coherence tomography (OCT) during a transient intraocular pressure (IOP) elevation to study lamina cribrosa deformation. Other research groups have measured the shape of the lamina cribrosa using a parameter termed the "lamina cribrosa curvature index" (LCCI) to indicate its biomechanical properties. Glaucomatous eyes were found to have a higher LCCI than healthy eyes. This study aimed to evaluate whether or not high myopes with weakened corneal biomechanics would have a weakened lamina cribrosa

To answer this question, the first study was conducted to confirm imaging of lamina cribrosa using the OCT during a transient IOP elevation as an appropriate method to be used. The second study evaluated the association between corneal biomechanics and lamina cribrosa.

IOP elevation has been used to examine lamina cribrosa biomechanics. A pilot study was conducted to determine if the IOP could be maintained at a stable high level through ocular compression while the lamina cribrosa was imaged. Inspired by the results of the pilot study, a decreasing trend of IOP during ocular compression and an extended study was conducted. The study included thirty high myopes with spherical equivalent ≤ -6.00 D and thirty low myopes with spherical equivalent from -0.50 D to

-3.00 D. The ocular compression phase and the recovery phase were 2 and 10 minutes, respectively. It was found that low myopes had slightly faster IOP declining rates during ocular compression than high myopes (LM: -3.25 mmHg/min; HM: -2.58 mmHg/min, p = 0.053). High myopes took longer than low myopes for IOP to sustainably return to their baseline levels (at 510 seconds versus at 360 seconds). This study concluded that IOP was unstable during ocular compression. Therefore, imaging the lamina cribrosa during the ocular compression did not apply to studying the shape of the lamina cribrosa. Given that the high and low myopes demonstrated different IOP changes during and after the ocular compression, it could be hypothesized that this phenomenon could be related to the different aqueous outflow facilities of the two groups. Further study is required to confirm this hypothesis.

To study the association between lamina cribrosa shape, LCCI was used. Thirty-two low (spherical equivalent from -0.625D to -3.00D) and thirty-two high (spherical equivalent ≤ -6.00D) myopes were recruited. The lamina cribrosa shape was imaged using a spectral domain OCT (Spectralis, Heidelberg, Germany) to derive the LCCI. A corneal indentation device was used to measure the corneal tangent modulus. Other corneal biomechanics parameters were measured using the Ocular Response Analyzer (ORA, Reichert Inc., USA). Low myopes had higher corneal tangent modulus (LM: 0.518 MPa; HM: 0.434 MPa, $p < 0.001$) and higher corneal hysteresis (CH) (LM: 10.45 mmHg; HM: 9.53 mmHg, $p = 0.012$), but higher LCCI (LM: 7.84; HM: 6.37, $p < 0.001$) values than high myopes. Although previous studies found a higher LCCI in glaucomatous eyes, LCCI may not be a good indicator of glaucoma risk of high myopes. This could be due to the lamina cribrosa being stretched during the axial elongation in myopic development.

Publications arising from the thesis

Paper published:

Xu, F. Y., & Lam, A. K. Association of corneal biomechanics and lamina cribrosa shape in myopia. Manuscript submitted.

Conference presentation:

Lam, A. K., & **Xu, F. Y.** (2020). Intraocular pressure change from ocular compression: a study of aqueous outflow facility. *Investigative Ophthalmology & Visual Science*, *61*(7), 4627.

Acknowledgements

TO MY CHIEF SUPERVISOR I would like to say a heartfelt thanks to Dr. Andrew Lam, for his patient guidance and advice throughout my time as his research student. Under his supervision, I learnt what is research work, and what is a responsible and consistent researcher. Without his continuous and kind support, I could not survive through the tough years in my MPhil life.

TO MY SUBJECTS Thanks for your help. The data taking in this study is hard as so many unexpected accidents happened, but you always support me. The completement of this research would not be smooth without your participation.

TO MY FRIENDS I really had a good life at PolyU with my friends, they helped me in research and life. I cherish the true friendship we have built and hope to support given to each other in the future. Best wishes to their future with wonderful adventures and satisfying endings.

TO MY FAMILIES Thanks to my family's support and encouragement for these three years. It was their love and hope that helped me to overcome the difficulties. The love from families helps me to walk in the path of life more peacefully.

XU Fangyu

TABLE OF CONTENTS

List of Abbreviations

AL	Axial length
ANOVA	Analyses of variance
BMO	Bruch's membrane opening
CCT	Central corneal thickness
CH	Corneal hysteresis
CI	Confidence interval
CID	Corneal indentation device
COVID-19	Coronavirus disease 2019
CRF	Corneal resistance factor
EDI	Enhanced Depth Imaging
E_N	Normalized corneal tangent modulus.
HM	High myopes
ICC	Intraclass correlation coefficient
IOP	Intraocular pressure
IOPcc	Corneal-compensated intraocular pressure
IOPg	Goldmann-correlated intraocular pressure
LC	Lamina cribrosa
LCD	Lamina cribrosa depth
LCCD	Lamina cribrosa curve depth
LCCI	Lamina cribrosa curvature index
LCCI_inf	LCCI in inferior mid-periphery plane
LCCI_mid	LCCI in mid-horizontal plane
LCCI_sup	LCCI in superior mid-periphery plane
LM	Low myopes
MPa	Megapascal
NTG	Normal tension glaucoma
OCT	Optical coherence tomography
OHT	Ocular hypertension
ONH	Optic nerve head

ORA	Ocular Response Analyzer
P1	First applanation pressure
P2	Second applanation pressure
PACG	Primary angle-closure glaucoma
POAG	Primary open-angle glaucoma
r	Pearson correlation coefficient
RGC	Retinal ganglion cells
R^2	Coefficient of determination
RMANOVA	Repeated-measures analysis of variance
RNFL	Retinal nerve fiber layer
SD	Standard deviation
SD-OCT	Spectral domain OCT
SER	Spherical equivalent refraction
Sw	Within-subject standard deviation
TRR	Test-retest repeatability

1. Introduction

1.1 Myopia

Myopia is a global health concern because of the rapid worldwide increase in its prevalence over recent decades. Myopia prevalence will continue to increase in the coming years. As estimated, there were over 108 million people with myopia in 2010, and 50% of the global population would be myopic by 2050, of which 10% would be high myopes (Holden et al., 2016; Morgan et al., 2012). In addition, myopia prevalence is at its highest in East and Southeast Asia (Chen et al., 2018; Rudnicka et al., 2016; Sankaridurg et al., 2021; Smith et al., 2009). The prevalence of myopia in school-aged children was observed to be higher in 2021 than in other years because of COVID-19 home confinement (Wang et al., 2021). Moreover, myopia is most commonly associated with axial elongation, but may be caused by an overly curved cornea and/or a cataractous lens with increased optical power (Flitcroft et al., 2019). Health, education, social activities, and financial burdens can all be adversely affected by the increasing prevalence of myopia (Sankaridurg et al., 2021; Saw et al., 1996).

1.1.1 Factors associated with myopia development

Generally, the onset and development of myopia are considered to be multifactorial. Myopia's development is affected by various unmodifiable factors, including age, genetics, and modifiable factors, like outdoor time, near work, and optical defocus. Multiple factors may jointly affect the incidence and progression of myopia.

1.1.1.1 Unmodifiable factors

Myopia appears to have a hereditary element. Various studies have reported the effect of genes and family history on myopia development. Epidemiological studies have shown that children with two myopic parents have a higher risk to inherit myopia than children with only one or no myopic parent (Ip et al., 2007; Li et al., 2022). However, it must be recognized that both genetics and behavior have roles in the family history

of myopia. Several gene variants have been shown to be associated with myopia and they are constantly increasing in number (Yu et al., 2011). An example is COL1A1, which is a gene affecting the content of type I collagen. Type I collagen exists in connective tissues, including the sclera, which supports the eyeball. Thus, any change in eye shape could be related to an alteration of type I collagen (Inamori et al., 2007). Another gene, PAX6, is also involved in high myopia by affecting eyeball morphogenesis (Tang et al., 2014). Therefore, identifying the myopia-related genes could further help in early myopia prevention.

Age is another unmodifiable factor in myopia development. The prevalence of myopia has increased annually in China since the introduction of a more intensive educational system (Li et al., 2022). The average age of myopia onset has decreased from 12 years of age in 1983 to 9 years in 2000 (Lin et al., 2004). The younger age of myopia onset has been associated with faster progression and a higher incidence of myopia in school children (Hyman et al., 2005; Saw et al., 2005). In addition, the proportion of high myopia has increased (Chen et al., 2018; Jones et al., 2012). As myopia can continue to progress until 20 years of age (Long et al., 2021), children with an earlier age of myopia onset would be more likely to develop high myopia with an extended period of myopia progression (Chua et al., 2016). Early-stage monitoring of refractive error and myopia control interventions in childhood are needed to control the progression to high myopia.

1.1.1.2 Modifiable factors

Hyperopic and myopic defocus may influence the development of myopia. This is because the optical defocus could stimulate the retina to move to the correct image plane by changing the choroidal thickness and vitreous chamber depth to change the axial length (AL) (Wang et al., 2016). Animal studies have confirmed that using hyperopic or myopic defocus with negative or positive lenses, respectively, could induce changes in the retinal plane (Arumugam et al., 2014; McFadden et al., 2014).

In human studies, an increase in AL and reduction of choroid thickness were associated with exposure to hyperopic defocus (Read et al., 2010). The use of dual-power lenses incorporating positive or plano power with negative power causing minimized spherical aberration, could reduce the progression of myopia (Dennis et al., 2007). Defocus-incorporated multiple segments spectacle lenses and defocus-incorporated soft contact lenses were developed for clinical use based on this finding. The central zone of these lenses was designed for clear distant viewing while incorporating the multifocal segments with positive power in the periphery area could simultaneously induce myopic to defocus and control the progression of myopia (Lam et al., 2020; Lam et al., 2014).

Although the association between near work and myopia has been controversial (Huang et al., 2015), most studies reported that a close reading distance, longer time spent on near work, as well as a small home environment could all increase the risk of developing myopia (Choi et al., 2020; Guo et al., 2013; Ip et al., 2008). Some studies have not found a significant correlation between time spent on near work and refractive error (Lin et al., 2014; Rose et al., 2008). It was observed that accommodation lag when responding to near targets could lead to hyperopic defocus, which could affect the development of myopia (Winawer et al., 2005).

Longer total time spent outdoors was associated with a lower rate and reduced risk of myopic progression (Cao et al., 2020; Dirani et al., 2009; Guo et al., 2013; Rose et al., 2008). It was hypothesized that the chromaticity of daylight with sufficient blue light could control myopia by altering the choroidal thickness (Foulds et al., 2013). In addition, high light intensity outdoors could inhibit eye growth (Feldkaemper et al., 2013; McCarthy et al., 2007; Zhang et al., 2020), by increasing the dopamine level which affects the choroidal thickness (Ashby et al., 2010; Zhou et al., 2017).

The level of sunlight and the viewing distances could be greater outdoors and the accommodation requirements could be smaller with more uniform dioptric space outside as compared with indoor activities. Thus, it was suggested that children should spend more time doing outdoor activities. Children in Taiwan who had 200 minutes or more of weekly outdoor time had significantly less myopic shift (Wu et al., 2018). Taiwan has implemented 120 minutes of outdoor activities daily during school time since 2010. The prevalence of reduced visual acuity has significantly decreased since the implementation of this activity (Wu et al., 2020). An increase in time for outdoor activities for the control of myopia progression has been confirmed and applied in the public health sector.

1.1.1.3 Corneal biomechanics: a new area

Corneal biomechanics is an important parameter associated with myopia development given that in vivo measurement is feasible. Properties of corneal biomechanics can be described by the relationship of the stress-strain curve through the corneal deformation. Two descriptors can be used to describe corneal biomechanical properties: elasticity (immediate deformation) and viscosity (dynamic deformation response). Elasticity is the instantaneous and reversible deformation of a material under an external load. Young's modulus (the ratio of stress to strain) is a parameter of elastic property reflecting the stiffness of a material (the resistance to hold force without deformation). Viscosity means that the rate of deformation is higher than the recovering rate in a material. The cornea behaves as a viscoelastic material, having both elastic and viscous properties to maintain corneal shape for stable vision and protect the internal structure of the eye (Figure 1.1).

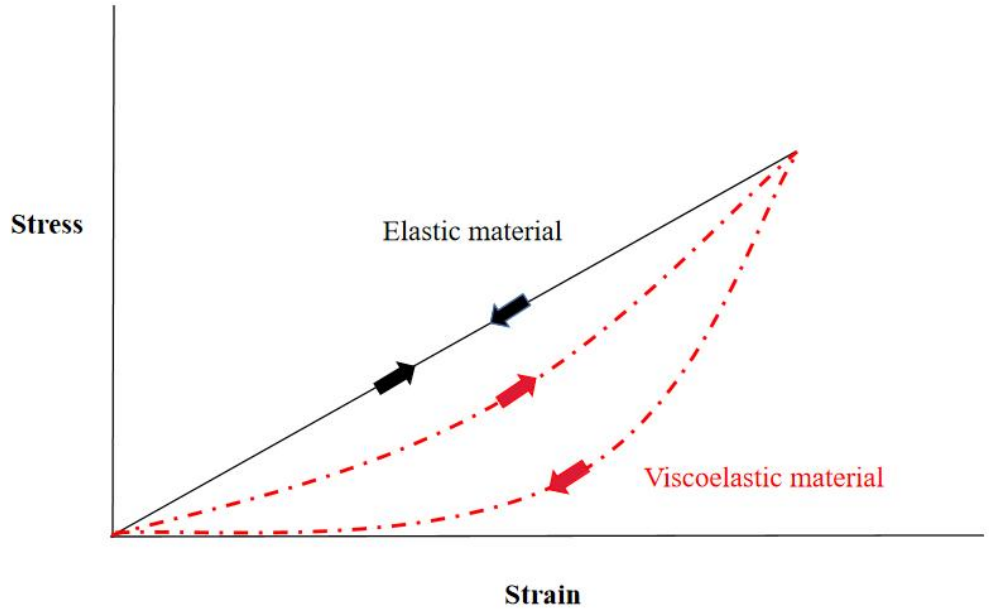

Figure 1.1. The stress-strain relationship of elastic and viscoelastic materials. The black solid line is for the elastic material, red dotted line is for the viscoelastic material. Upward and downward arrows mean loading and unloading, respectively.

The Bowman's membrane, corneal stroma (accounting for 90% thickness), and the Descemet membrane all consist of collagen fibers (types I, III, and V) (Silver et al., 2018). The biomechanical properties of the cornea are mainly determined by the stromal layer (Ma et al., 2018). There are intervals found between the collagen fibrils, which are filled with a gel-like matrix formed from proteoglycans combined with water (Müller et al., 2004). The proteoglycan matrix may contribute to the viscosity of the cornea as it is fluid-like, thereby allowing energy absorption by sliding between molecules and fibrils (Silver et al., 2018). Moreover, the orientation of collagen fibrils in the corneal stroma can be both vertical and horizontal in the central cornea but run circumferentially around the limbus (Meek et al., 2004). This collagen fibril orientation allows the cornea to have elasticity because it provides the strength of resistance to deformation.

Corneal hysteresis (CH) and corneal tangent modulus are two descriptors of the viscoelastic property of the cornea. Hysteresis represents the ability of energy dissipation. The area between the two dotted curve lines in Figure 1.2 represents hysteresis (Figure 1.2). Corneal elastic tangent modulus refers to an instant and reversible deformation of the cornea under an external load and can be represented as the instantaneous slope at a specific load on a stress-strain curve (Figure 1.3). Lam et al. (2015) reported that the corneal tangent modulus had good repeatability (coefficient of variation = 7.34%, intraclass correlation coefficient (ICC) = 0.84). Hon et al. (2016) demonstrated that the tangent modulus was stable throughout the day by studying the tangent modulus of young adults from 09:00 am to 9:00 pm at 3-hour intervals. In addition, the tangent modulus showed significant regional differences along the horizontal meridian of the cornea (Hon et al., 2017).

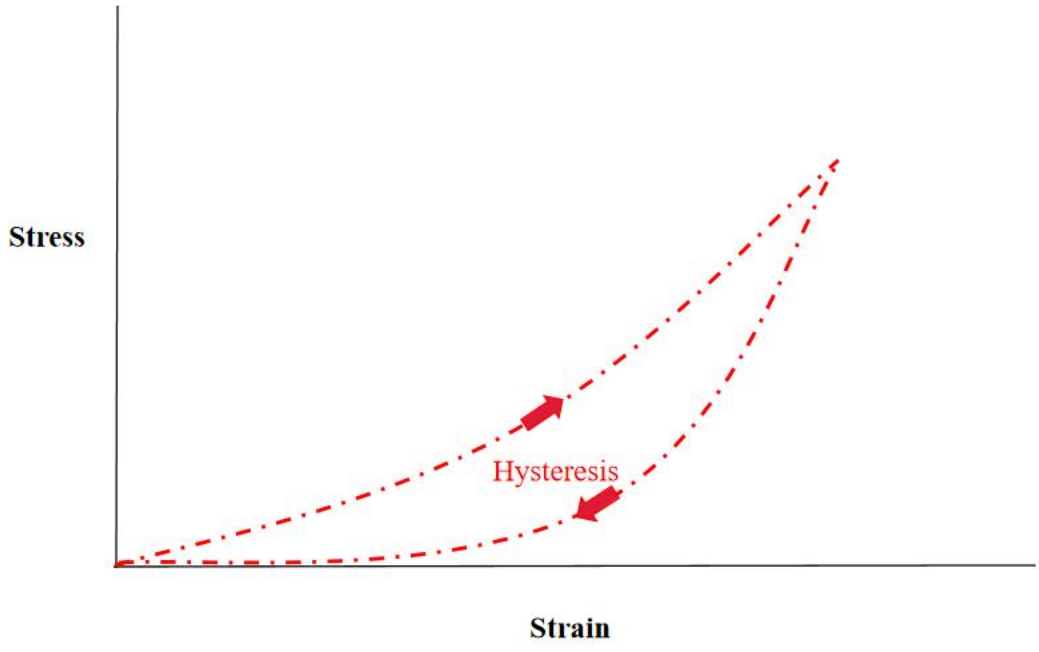

Figure 1.2. The stress-strain relationship in viscoelastic materials. The area between the two red dotted lines is the hysteresis. Upward arrow indicates loading, downward arrow is unloading.

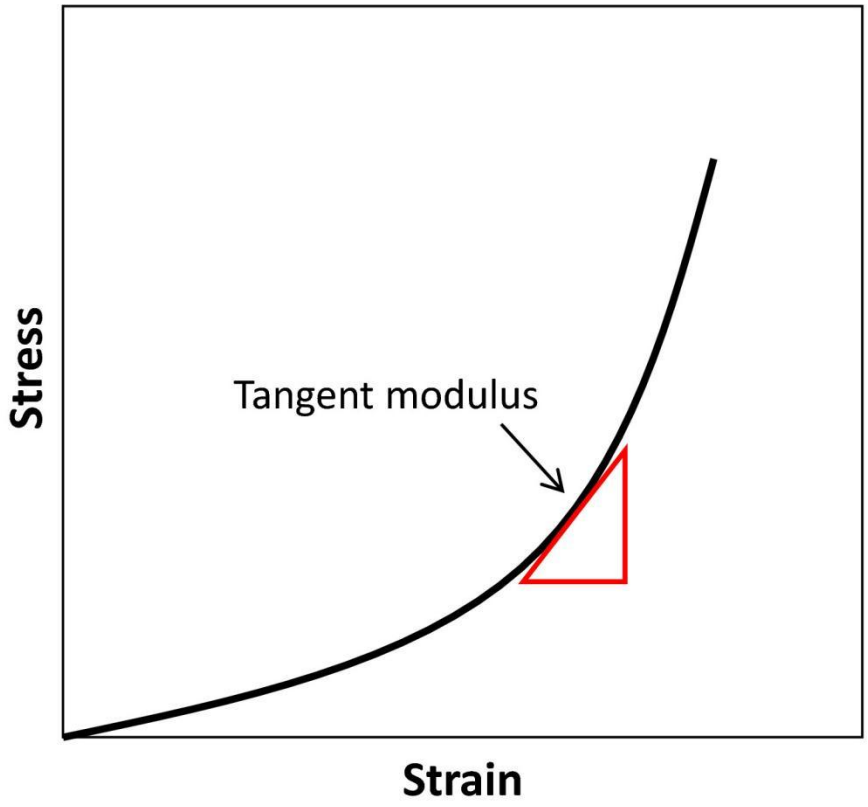

Figure 1.3. A typical nonlinear curve showing the definition of tangent modulus (Hon et al., 2017). The tangent modulus can be calculated as the immediate slope of the stress-strain curve.

According to the study of (Chang et al., 2001), the cornea became thinner during axial elongation. A longer eyeball with a thinner cornea contains less extracellular matrix, which may lead to weaker viscoelastic properties (Garcia-Porta et al., 2014). Previous studies have found that CH had a negative association with AL (Bueno-Gimeno et al., 2014; Plakitsi et al., 2011; Shen et al., 2008), in contrast, few studies reported no correlation between CH and myopia (Lim et al., 2008). The inconsistency may be due to the multiple effects of central corneal thickness (CCT, positive correlation) and cornea curvature on CH (negative correlation) (Lim et al., 2008; Shah et al., 2006). However, some studies reported that CCT did not influence CH in myopic eyes (Al-Mezaine et al., 2009; Fam et al., 2006). Thus, it was speculated that it was not the thickness but the altered corneal shape or its content during myopia development that

resulted in the different corneal biomechanics observed in myopic eyes (Dong et al., 2018). A recent meta-analysis (Wu et al., 2019) also supported this hypothesis.

Some studies using corneal tangent modulus estimation confirmed that highly myopic eyes had weaker corneal biomechanics. In an animal study, chicks with higher myopia had a lower corneal tangent modulus (Kang et al., 2018). In a clinical study, high myopes displayed a significantly lower corneal tangent modulus than low myopes (Hon et al., 2017).

1.1.2 High myopia-associated ocular problems

Pathologic myopia has a high prevalence of occurring in highly myopic eyes and can result in irreversible blindness (Verkicharla et al., 2015). It has been reported that Asians had the highest prevalence of pathologic myopia (Wong et al., 2014) and the prevalence could increase with age (Wong et al., 2016). Although most epidemiological studies have defined "high myopia" as a spherical equivalent of at least –6.00 D (Flitcroft et al., 2019), currently, there is no official definition of pathologic myopia. The presence of a posterior staphyloma is an important marker for pathologic myopia (Ohno-Matsui, 2016).

Pathologic myopia may be defined as excessive axial elongation causing structural changes in the posterior segment of the eye (sclera, choroid, and retina), accompanied by visual impairment (Ohno-Matsui, 2016). Complications from high myopia are leading causes of severe visual impairment (Van Newkirk, 1997; Wong et al., 2014), including maculopathy, posterior staphyloma, cataract, and glaucoma (Cho et al., 2016).

1.1.2.1 Glaucoma

Glaucoma is one of the leading causes of irreversible blindness in the adult population worldwide (Quigley et al., 2006). It is characterized by the loss of retinal nerve fiber

layer (RNFL) tissues (or neuroretinal rim) in the optic nerve head (ONH), including the death of retinal ganglion cells (RGC), thereby leading to visual field loss. The glaucomatous damage in the neuroretinal rim of ONH is termed as glaucomatous optic neuropathy (Gupta et al., 1997).

Studies have revealed that the levels of myopia were positively associated with the prevalence of primary open-angle glaucoma (POAG) (Mayama et al., 2002). Moderate-to-high myopes had a 2–3-fold increased risk of glaucoma as compared with the emmetropes (Mitchell et al., 1999). In contrast, hyperopic eyes, which have shallower anterior chamber depth and more anteriorly positioned lens, increased the risk of a pupillary block to induce primary angle-closure glaucoma (PACG) (Wright et al., 2016). POAG progresses faster in high myopes than in eyes of other myopes, it was confirmed by comparing the progression of visual field loss (Lee et al., 2008). However, Lee et al. (2015) reported that there was no association between myopia and the progression of POAG. This discrepancy may be due to some studies using refractive error to categorize myopic subjects instead of AL. The ONH structures in longer eyeballs may be more susceptible to elevated intraocular pressure (IOP), thereby causing glaucomatous damage (Chen et al., 2012).

1.1.2.2 Maculopathy

The frequency of myopic macular degeneration has increased rapidly worldwide (Bourne et al., 2018), particularly in Asia (Wong et al., 2021). Myopic macular degeneration could affect over 47% of high myopes (Zou et al., 2020). If myopia progresses to -10 D, the risk of developing maculopathy is increased to approximately 14-fold (Leveziel et al., 2020). Progression of myopic macular degeneration in high myopes older than 40 years may reach 40% (Hayashi et al., 2010; Li et al., 2019). Typical signs include: retinal, choroidal, and scleral thinning, as well as choroidal neovascularization, chorioretinal atrophy, tractional damage near the macula, the concave shape of the sclera, and Bruch membrane holes at the macula (Ruiz-Medrano

et al., 2019). The posterior pole could be stretched because of axial elongation. Scleral ectasia may result in macular photoreceptor damage and hence the central visual loss. Due to the changes associated with high myopia, it is suggested that patients with high myopia should undergo a detailed investigation, possibly including ocular biomechanics.

1.1.2.3 Cataract

Another common complication of high myopia is cataract. The types of incident cataracts included nuclear, cortical, and posterior subcapsular cataracts. Population-based studies have shown that refractive errors may be the main risk factor for the incidence of cataracts, particularly nuclear and posterior subcapsular cataracts (Haarman et al., 2020; Pan et al., 2013), with high myopes having more than threefold and sevenfold risks for nuclear and posterior subcapsular cataract, respectively, than the emmetropes (Kanthan et al., 2014). A 5-year follow-up study reported that there was a strong correlation found between myopia and the progression of incident cataracts (Wong et al., 2001). The biological mechanism was proposed to be increased exposure of the crystalline lens to oxygen resulting in the production of lipid peroxidation by-products, which could further lead to lens opacity (Micelli-Ferrari et al., 1996). The peroxidation by-products inducing lens opacity were higher in the crystalline lens of high myopes than in the emmetropes (Boscia et al., 2000; Micelli-Ferrari et al., 1996). More oxygen can be transported from retinal vessels to the crystalline lens when the vitreous gel is liquefied (Holekamp, 2010), and this liquefaction increases with myopia (Holekamp et al., 2008). This may be the reason why posterior subcapsular cataract occurs more frequently than cortical cataracts in myopes. Hence, posterior subcapsular cataract could be considered a typical secondary pathological change of high myopia.

1.2 Primary open-angle glaucoma (POAG)

In recent decades, the worldwide population of POAG has increased from around 45 million patients in 2010 to around 59 million by 2020 (Quigley et al., 2006). More than 79.76 million people worldwide would have POAG by 2040, as estimated by (Tham et al., 2014).

1.2.1 Pathological mechanisms of POAG

Although the specific pathophysiological mechanisms of RGC death in glaucoma remain unclear, two theories for its development, the mechanical and vascular have been proposed (Fechtner et al., 1994).

The lamina cribrosa (LC) is part of the posterior sclera and may be a weak point because of the discontinuity of the corneal-scleral shell in the eyeball (Huang et al., 2013; Quigley et al., 1983). The LC is like an hourglass-shaped with RGC axons and retinal blood vessels passing through the pores. The nourishment or intracellular content could be transported by axons within the LC. When damage occurs to the LC, axonal transportation may be disturbed leading to RGC death. Meanwhile, the LC experiences a translaminar pressure gradient (around 20–30 mmHg/mm) induced by a relatively high IOP and low retrobulbar cerebrospinal fluid pressure (Morgan et al., 2016). Therefore, the LC is one of the sites of glaucomatous damage.

The mechanical theory hypothesized that the elevated IOP acts as a force from inside to outside to compress the LC, causing it to bow outward. A second force emanates from raised sclera tension pulling on the perimeter of the LC sheets. Both forces could distort the LC and adversely influence the axoplasmic transport within the RNFL, which may lead to the death of RGCs and their axons resulting in the thinning of rim tissues and deformation of the ONH (Fechtner et al., 1994; Quigley, 1987).

The vascular theory suggests that the loss of RGC in glaucoma is attributable to insufficient blood flow to the ONH. This could be the result of either a high IOP or other causes that affect the ocular blood supply (Flammer et al., 2002; Quigley et al., 1989). For example, decreased diastolic perfusion pressure and elevated systemic blood pressure increase the risk of developing glaucoma (Bonomi et al., 2000). This mechanism could be consistent with a new population-based study demonstrating a negative association between the diastolic perfusion pressure and the rate of RNFL loss (Jammal et al., 2022). Although IOP elevation has still been considered as the major risk factor, there has been increasing evidence that supports the role of vascular risk factors in the pathogenesis of glaucoma (Cantor et al., 2018; Flammer, 1994).

Recently, a biomechanical theory (Figure 1.4) has been proposed. Stress at the ONH could be induced by the translaminar pressure gradient between the IOP and the retrobulbar cerebrospinal fluid pressure through the anterior and posterior LC. In addition, the strain could be reflected by a change in the load-bearing connective tissue of the LC and intracellular components (astrocytes, endothelial cells). The IOP-induced stress-strain response could lead to several downstream pathogenic pathways, that lead to a combination of both mechanical and vascular theories resulting in nerve damage (Downs et al., 2008; Tan et al., 2018).

In conclusion, although there are several pathological theories presented, IOP and blood flow are the two primary widely accepted etiological factors.

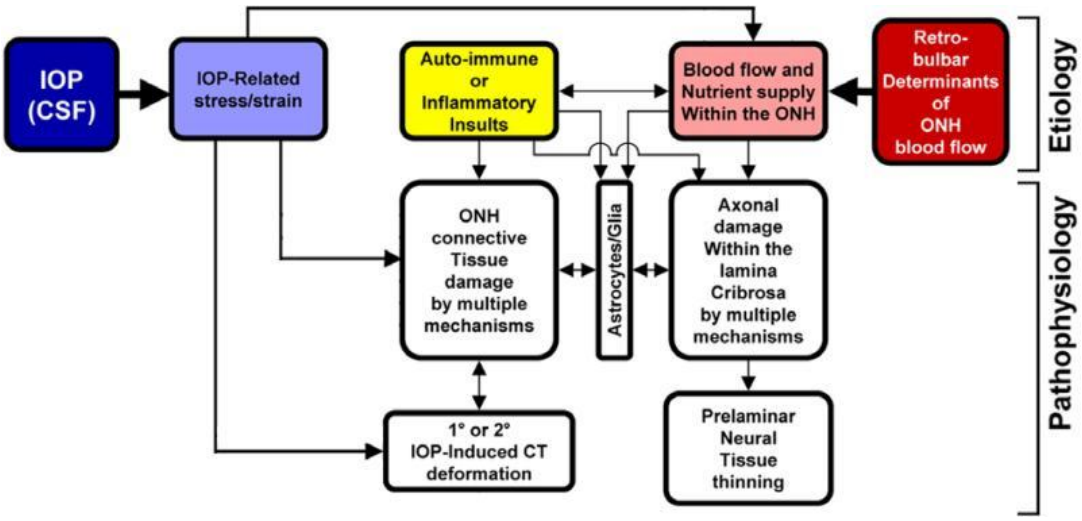

Figure 1.4. The biomechanical paradigm (Downs et al., 2008).

1.2.2 Factors associated with progression of POAG

1.2.2.1 Intraocular pressure

High IOP is one of the most important risk factors for the development of glaucoma. Previous studies have established that lowering the IOP could delay and decrease the risk of glaucomatous damage. Glaucoma progression is significantly delayed by reduction of IOP by 5.1 mmHg through trabeculoplasty or medication (Heijl et al., 2002). Similarly, it was determined that every 1 mmHg of reduction in IOP could result in a 10% decrease in glaucoma progression (Leske et al., 2003).

However, the mean and peak variations of IOP have been investigated as predictors for glaucoma development. Some studies reported that IOP fluctuation between visits could influence the progression of glaucomatous damage. For example, 1 mmHg elevation in IOP could increase the risk by 4–5 times (Lee et al., 2007). Rao et al. (2013) reported that progression would be increased by around 0.4% per year with each one mmHg IOP fluctuation. They also reported found that only long-term IOP variation between follow-ups could predict glaucoma progression, rather than the mean or peak variations of IOP. An 8-year follow-up study reported contrary findings,

which found that the mean IOP value was significantly associated with the development of glaucoma rather than long-term IOP fluctuation, but there was a small effect of the mean IOP value (hazard ratio was 1.1) (Bengtsson et al., 2007). Asrani et al. (2000) reported that diurnal IOP fluctuation (difference between the highest and lowest IOP over the course of 24 hours) had a significant association with glaucoma development rather than the baseline mean IOP. Apart from the short-time IOP fluctuation, the peak IOP was also associated with the risk of glaucoma progression rather than long-term IOP (Matlach et al., 2019). However, Wang et al. (2011) did not find any significant difference among peak, mean, and short-time fluctuation of IOP between glaucoma and healthy subjects. It has been suggested that long-term IOP fluctuation was more important than mean IOP regarding the susceptibility to glaucomatous damage (Caprioli et al., 2008). Jonas et al. (2007) demonstrated that the IOP could influence the rate of glaucoma progression rather than its amplitude.

In summary, the IOP is a variable parameter affected by multiple factors (aqueous humor dynamics and body positions, etc.), which might lead to inconsistent conclusions (Sit, 2014). However, it is without doubt that IOP should be considered as an important risk factor for glaucomatous damage.

1.2.2.2 Corneal hysteresis

Morphologically, the shape of ONH is related to the CH. Eyes with greater optic cup depth and larger cup-to-disc ratio have lower CH (Prata et al., 2012). Eyes with higher LC curvature (Lee et al., 2019) and less LC deformation also have lower CH (Lanzagorta-Aresti et al., 2017). Eyes with higher CH have a greater ability to absorb and dissipate energy. Therefore, those eyes have less susceptibility to glaucomatous damage. The CH of POAG and normal tension glaucoma (NTG) was reported to be lower than that of healthy people (Abitbol et al., 2010; Grise-Dulac et al., 2012; Morita et al., 2012; Sayin et al., 2021), whereas the difference between POAG and NTG was inconclusive (Ang et al., 2008; Shah et al., 2008). Various studies showed

that eyes with ocular hypertension (OHT) had higher CH than glaucoma (Kaushik et al., 2012; Rojananuangnit, 2021), indicating a greater tolerance to high IOP in OHT. In addition, CH in medically-treated POAG showed a continuous rise (Tsikripis et al., 2013). On the contrary, a decrease in CH indicated a progression of visual field defects (De Moraes et al., 2012; Medeiros et al., 2013). Some practitioners have used CH to aid the diagnosis of POAG. Schweitzer et al. (2018) applied 10 mmHg CH as a cutoff point with good accuracy to distinguish moderate-severe glaucoma. Hence, it is possible that the CH can be a good indicator of POAG progression.

1.2.2.3 Lamina cribrosa

The LC is one site of glaucomatous damage (Quigley et al., 1981). Deformation of LC (such as elongation and decreased size of pores, or backward bowing) appear prior to visual field defects in glaucoma (Quigley et al., 1983; Wang et al., 2013). Therefore, it is necessary to study the morphological changes of the LC for the early diagnosis of glaucoma.

Some morphological parameters of the LC could have potential clinical applications. Spectral-domain optical coherence tomography (SD-OCT) is commercially available to capture the LC structure. Individuals with a thick LC might be less susceptible to glaucomatous neuropathy. Healthy people had a thicker LC than glaucoma patients, and the reduction of LC thickness was correlated with the severity of glaucoma (Park et al., 2012; Park et al., 2013).

The lamina cribrosa depth (LCD) is a parameter used to describe the maximum distance from the anterior LC surface to the Bruch's membrane opening (BMO) level (Lee et al., 2013) (Figure 1.5). Mean LCD was reported as 422 μm in healthy Chinese people and independent of IOP and AL (Tun et al., 2021). It was found that LCD was greatest and lowest at its superior and the central ONH, respectively (Seo et al., 2014). POAG patients had a larger LCD than healthy people with posterior displacement and

thinning of the LC caused by IOP elevation (Lee et al., 2017). However, LCD measurement can be influenced by choroidal thickness (Johnstone et al., 2014; Kim et al., 2019). Choroidal thickness can be mistakenly interpreted as part of the LCD (Tun et al., 2021). For example, an eye with a thicker choroid has a greater LCD even though the eye does not have a very curved LC (Lee et al., 2017). Hence, it is more accurate to measure the LCD from the scleral plane (Vianna et al., 2017), but clearly identifying scleral plane remains limited by current clinical image techniques.

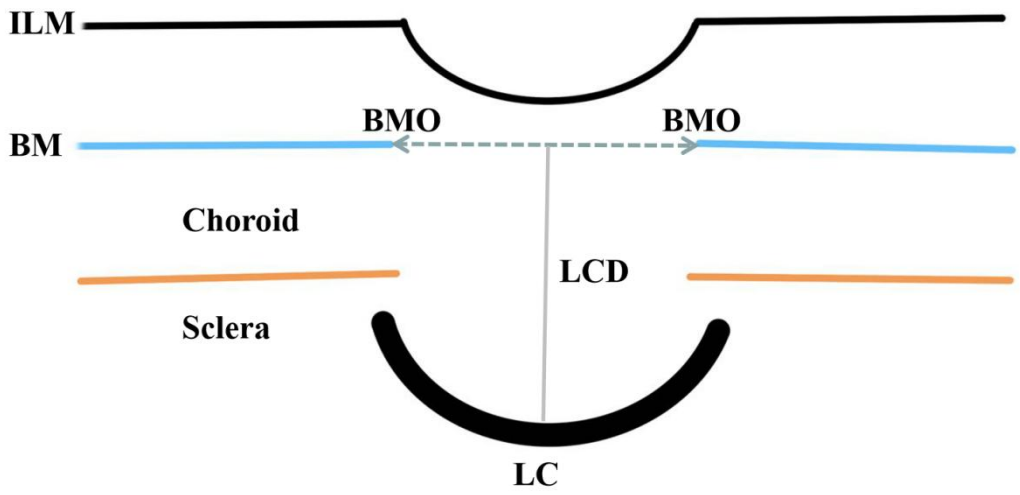

Figure 1.5. Diagram of the LCD measurement. The gray dotted line indicates the BMO level. Orange line indicates the chorioscleral interface. The distance between the BM and the chorioscleral interface is the choroid. LCD is the maximum depth from the BMO level to the anterior LC surface. ILM: Internal limiting membrane; BM: Bruch's membrane; BMO: the opening of BM; LC: lamina cribrosa.

Recently, the lamina cribrosa curvature index (LCCI) as a new parameter, has been used to indicate the morphological changes of the LC. It has been suggested that LCCI is better than the LCD in characterizing the morphological changes of the LC (Kim et al., 2019; Lee et al., 2017). LCCI also had a stronger correlation with the RNFL thinning than the LCD to predict RNFL progression in POAG (Lee et al., 2018). LCCI represents the LC curvature without the influence of choroidal thickness.

In the central area, the LCCI is at its minimum, but becomes larger in the superior and inferior ONH (Kim et al., 2020). It was reported that higher IOP, older age, and shorter AL were correlated with larger LCCI (Lee et al., 2019). Lee et al. (2017) proposed that an LCCI of 9.51 could be the threshold to induce axonal damage. POAG and NTG patients had higher LCCIs than healthy subjects (Kim et al., 2020; Kim et al., 2019). In addition, the LCCI was positively correlated with the rate of RNFL thinning in patients with suspected glaucoma and POAG eyes (Kim et al., 2018; Lee et al., 2018). LCCI is useful even in glaucoma without IOP elevation. In patients with unilateral NTG, eyes with NTG had greater LCCI than in a healthy person's normal eyes (Kim et al., 2019). This indicated that LC strain could be involved even if the IOP was not high. Eyes with a higher LCCI could be more susceptible to glaucomatous damage. Kim et al. (2020) found that LCCI was greater in the NTG than in the healthy subjects. They further proposed that LCCI could reflect the mechanical strain of the ONH. The smaller LC vessel density in NTG with a higher LCCI could affect ONH perfusion caused by the collapse of lamina capillaries. Comparing eyes with NTG with non-arteritic anterior ischemic optic neuropathy, Kim et al. (2020) found that LCCI was significantly greater in the NTG than in the non-arteritic anterior ischemic optic neuropathy patients who had LCCIs similar to healthy controls. Therefore, LCCI could help differentiate LC deformation associated with glaucoma. These findings supported the hypothesis that posterior LC bowing is a characteristic of different kinds of glaucoma. LCCI could be used as a valid parameter to describe the ONH deformation related to glaucoma.

The LC global shape index is also used to represent LC morphology. It is a derived parameter used to indicate the geometrical shape of the whole LC rather than just along one meridian (Kadziauskienė et al., 2018). Unlike LCCI or LCD, global shape index is independent of the BMO reference plane. Global shape index values vary from -1 (posteriorly curved LC) to +1 (anteriorly curved LC), and the most common global shape index in healthy eyes is -0.34 (Thakku et al., 2015). A comparison of LC

global shape indexes of OHT, POAG, and healthy people revealed that those with POAG had the lowest result, indicating more posterior deformation. The LC global shape index is a single quantitative index used to categorize different diseases associated with different levels of deformation (Tun et al., 2016).

For better understanding of the pathogenesis of glaucoma, clinical studies have investigated the mechanical response and morphological changes of the LC through acute IOP elevation (Agoumi et al., 2011; Beotra et al., 2018; Sigal et al., 2014; Tun et al., 2016). These studies used ophthalmodynamometry to increase IOP through ocular compression. Morphological changes of the LC were monitored by SD-OCT during 1–2 minutes of acquisition. For example, the LC in glaucomatous eyes had more posterior movement under a similar IOP rise as compared with the normal eyes (Bellezza et al., 2003). Beotra et al. (2018) found different LC displacements among POAG, OHT, and normal subjects through an ocular compression to increase IOP to around 35 and 45 mmHg. Given that OHT eyes had lower IOP-induced deformation than healthy and glaucoma eyes, OHT eyes may have stronger tissue biomechanics to resist high IOP. This argument coincides with a previous finding that OHT patients had higher CH than those with glaucoma. Therefore, high IOP did not adversely affect the LC in OHT.

Therefore, eyes with glaucoma are often characterized by morphological changes in the LC due to elevated IOP (Midgett et al., 2020). This indicates altered LC biomechanical properties in glaucoma based on the relationship between stress (increased IOP) and strain (LC deformation).

1.3 Biomechanics relationship between myopia and POAG

1.3.1 Relationship of corneal hysteresis between myopia and POAG

Myopia is mainly due to axial elongation which involves structural changes, such as thinning of the sclera (McBrien et al., 2003; Rada et al., 2006) and the cornea (Chang

et al., 2001). Eyeball elongation is accompanied by narrowing and disconnection of collagen fibers, as well as a reduction in the fibril diameter (McBrien et al., 2001). The tensile strength of the corneal tissue could be lower (Yang et al., 2009). High myopes had thinner sclera (Rada et al., 2006) and thinner corneas, which would be more deformable (He et al., 2017). Therefore, as mentioned in previous section, CH was lower with higher AL.

The cornea, sclera, and LC are continuous structures developed from the mesoderm. The viscoelastic properties of sclera and cornea have been studied (McBrien et al., 2009). Their biomechanical properties could be related due to the similar component of the extracellular matrix (Albon et al., 1995; Meek et al., 2001; Sawaguchi et al., 1993). It was expected that the cornea could reflect the glaucomatous damage as it had similar biomechanical properties to the LC. Clinically, alteration of the CH in POAG has been thoroughly covered in Section 1.2.2.2. Corneal modulus was slightly lower in the glaucoma group than in the healthy group (Xu et al., 2022), meanwhile, high myopes had softer cornea than the emmetropes (Hon et al., 2017).

In short, eyes had weaker biomechanical properties, which is also associated with more rapid glaucomatous damage. The biomechanical changes in the cornea caused by axial elongation have the potential to impact on the biomechanics of the posterior sclera and LC affecting the incidence of glaucoma, due to their similar biological composition.

1.3.2 Relationship of lamina cribrosa between myopia and POAG

The structures of the LC provide support to RGC axons and protects them under an increased pressure gradient. When the LC is thin, the pressure gradient (stress) at the LC is high, that is the difference between the IOP and retrobulbar cerebrospinal fluid pressure (Morgan et al., 2016). A thin LC could have low viscoelastic properties due to altered collagen fibers which require higher strain to resist the stress (Voorhees et

al., 2017). A thin LC could also have lower elastic properties resulting in permanent deformation of the LC and irreversible cupping at the ONH (Spoerl et al., 2005).

Previous mentioned studies have reported that axial elongation results in weaker corneal biomechanics. It it is possible that the LC and the cornea have similar biomechanical properties due to their similar collagen fiber content, and the LC biomechanical strength would be reduced during the axial elongation. Therefore, high myopes have higher risks of glaucomatous damage. However, the biomechanical linkage between the LC and cornea through the sharing of similar collagen content has remained as a theoretical hypothesis without any clinical experimental proof, which forms the knowledge gap of this project.

1.4 Research question and hypothesis

The research question of this project based on the above clinical and biological findings is "should high myopes with weakened corneal biomechanics have a weakened LC"? It is hypothesized that there is an association between corneal biomechanics and LC shape.

Two clinical studies were conducted in this project to evaluate the hypothesis:

Study 1: Evaluation of intraocular pressure changes from the ocular compression

1) To monitor IOP before, during, and after the ocular compression
2) To compare IOP before, during, and after the ocular compression between different myopic groups

Study 2: Association between corneal biomechanics and lamina cribrosa shape

1) To investigate the relationships between corneal biomechanical parameters and LC morphology
2) To compare any difference between high and low myopes

2. Study 1: Evaluation of intraocular pressure changes from ocular compression

Although it is now clinically feasible to measure corneal biomechanics and assess the morphology of the LC using SD-OCT, there have been limited studies to investigate and compare the characteristics of the two tissues together. Some clinical studies investigated the morphological changes in the LC during the transient IOP elevation (Agoumi et al., 2011). Ocular compression was used to increase IOP, and the ONH was imaged during IOP elevation. IOP was measured immediately after the ocular compression with no further monitoring during and after OCT imaging.

However, several studies of LC morphology using ocular compression assumed that the IOP was stable during two minutes of ONH acquisition (Tun et al., 2016; Zhang et al., 2020). Hence, a study has planned to investigate whether or not IOP was stable during the ocular compression.

2.1 Methodology

2.1.1 Subjects

Based on literature reviews (Bedggood et al., 2018; Chen et al., 2020; Elsheikh et al., 2015), the number of healthy subjects participating in studies with ocular compression was around 7–25. In a pilot study, at least 30 healthy subjects were recruited. Based on results of the pilot study, an extended study was conducted to include 30 low myopes and 30 high myopes. Healthy young adults with different myopia status were recruited within the university campus. The current study was performed according to the tenets of the declaration of Helsinki and approved by the Human Subjects Ethics Committee of The Hong Kong Polytechnic University. Informed consent was obtained from each subject prior to any eye measurements.

The inclusion criteria of the pilot study were as follows:

a. Chinese aged between 20-30 years
b. No history of ocular disease, trauma, or surgery
c. Currently not taking any medication
d. Myopia, with spherical equivalent refraction (SER), < -0.50 D in both eyes
e. Distance visual acuity of at least LogMAR 0.00 in each eye

Inclusion criteria of the extended study were as follows:

a. Chinese aged between 20-30 years
b. No history of ocular disease, trauma, or surgery
c. Currently not taking any medication
d. Low myopes (-3.00D ≤ SER ≤ -0.50D) in both eyes, and high myopes (SER ≤ -6.00D) in both eyes
e. Distance visual acuity of at least LogMAR 0.00 in each eye

Exclusion criteria were listed as follows:

a. IOPcc or IOPg > 21 mmHg
b. Waveform score < 3.6 from the Ocular Response Analyzer (ORA, Reichert Inc., USA)
c. Contact lens wearing

2.1.2 Apparatus and procedures

As the ophthalmodynamometer is no longer commercially available, a phosphene pressure tonometer (Proview™, Figure 2.1) was modified to artificially increase the IOP. Originally, Proview™ was used by patients as a tonometer to self-monitor their IOP (Lam et al., 2004). It is a spring compression device consisting of a spring-loaded plunger with a flat applicator.

Modification of the Proview™ included extending the front part of the device (Figure 2.1). The force provided by this modified Proview™ was linear to the scale. It had good inter-examiner reproducibility and intra-examiner repeatability for ocular compression (Lam et al., 2019). The modified Proview™ was applied in the right eye through the lower eyelid at the temporal side. An electronic circuit was added at the other end of the Proview™. A beep tone was given when compression reached the pre-set scale (equivalent to force around 47 g). Afterward, another beep tone at a higher pitch was given as a reminder if the compression exceeded this scale.

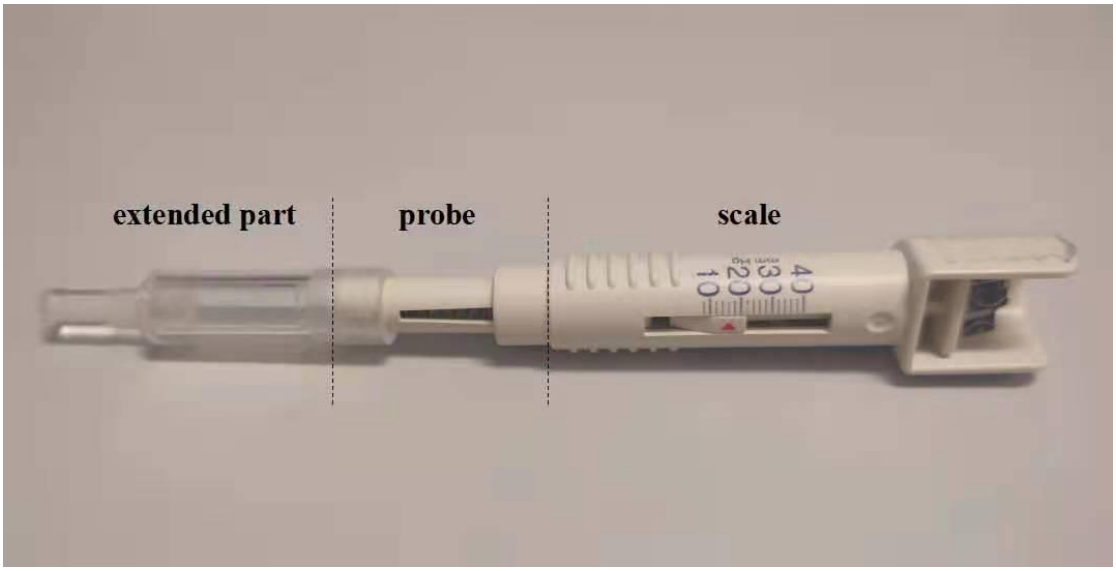

Figure 2.1. The components of the Proview™ after the modification. The modified Porview™ included an extended part with a 6 mm diameter probe. The scale was in increments of 2 mmHg.

All measurements were conducted from 9:00 am to 1:00 pm to avoid the diurnal fluctuations of IOP and only the right eye was selected for each subject. A pilot study initially recruited 34 young myopes with refractive errors measured using an open-field auto-refractor (ARK-510A, Nidek Co., Ltd., Japan) followed by visual acuity measurement. AL was measured by the IOL master 500 (Carl Zeiss Meditec AG, Germany). IOP was measured using rebound tonometry (iCare, Tiolat, Finland). The

modified Proview™ facilitated ocular compression was performed by the subjects themselves (Figure 2.2). IOP readings were recorded by the rebound tonometer at 30-second intervals throughout the study, i.e., time-zero, time-30S, and time-60S.

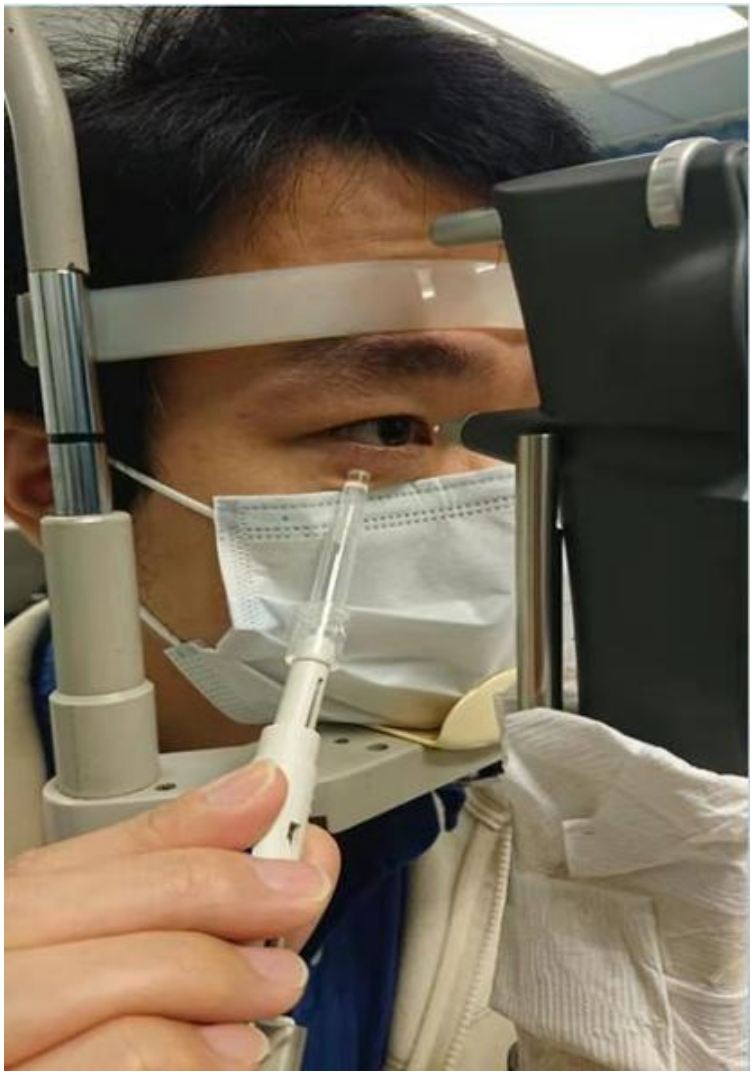

Figure 2.2. The use of the Proview™ by a subject. The modification facilitated ocular compression performed by the subject himself.

Before compression, three IOP values were recorded as a baseline within one minute. Then, IOP readings within one minute were measured as C-0S, C-30S, and C-60S, from the beginning of the ocular compression. IOP was measured immediately after the ocular compression and during a recovery phase for five minutes, termed as R-0S,

R-30S, until R-300S.

As the results (shown in the results section) from the pilot study were unexpected, an extended study was conducted. This involved an equal number of subjects in the low and high myopia groups. The compression time was extended from 1 minute to 2 minutes and the recovery phase to 10 minutes. The modified Proview™ was mounted on a head and chin rest (Figure 2.3). ORA (Reichert Inc., USA) measurements were conducted at baseline with three acquisitions, each with a waveform score of ≥ 3.6.

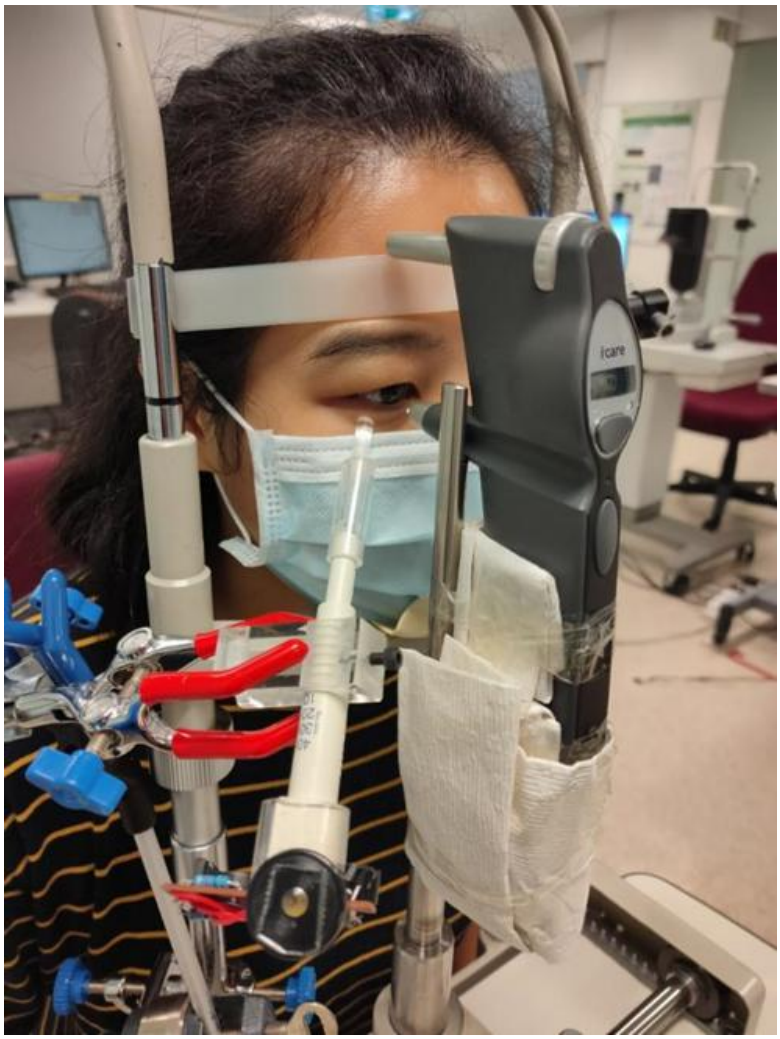

Figure 2.3. A mounting device used to keep stable force. The modified Proview™ was mounted on a head and chin rest.

2.1.3 Measurement of corneal hysteresis

The CH is a biomechanical parameter representing the viscoelastic properties of the cornea (Piñero et al., 2014). Clinically, it can be obtained by the ORA (Figure 2.4), which contains an infrared light emitter, an infrared sensor, an air pump, and a pressure transducer. During an ORA measurement, a light beam produced by the infrared light emitter aligns with the center of the cornea and is subsequently monitored by the infrared sensor. When the cornea is applanated, the amount of reflected light would reach its maximum and be detected by the infrared sensor. The first applanation pressure is then obtained (P1). The air puff further pushes the cornea inward producing a concave indentation. Then the cornea returns to a second applanation state, with the second applanation pressure (P2) before returning to its original shape (Figure 2.5) (Luce, 2005).

Figure 2.4. The Ocular Response Analyzer (ORA). The ORA contains an infrared light emitter, infrared sensor, air pump, and pressure transducer.

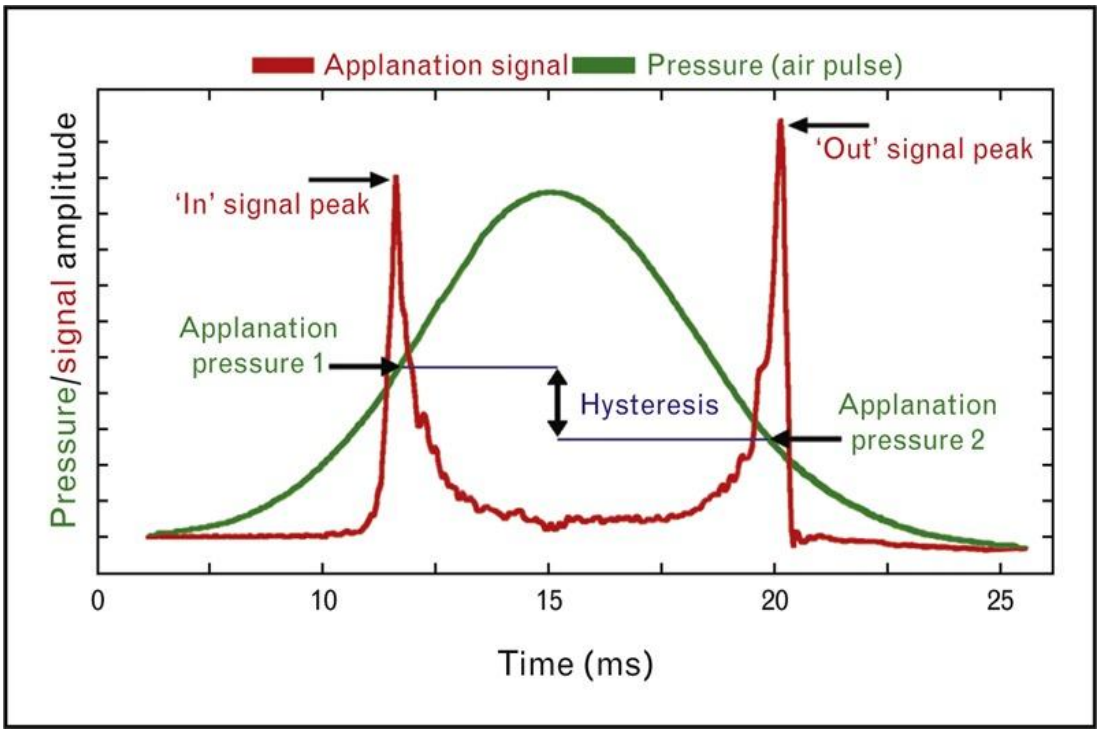

Figure 2.5. A typical applanation-pressure plot was adopted from the instruction manual of the ORA (Reproduced by courtesy of Reichert Inc., USA). Two peaks in the red line refer to the inward and outward states of the cornea, respectively.

The following parameters are provided.

a) CH refers to the difference between the two applanation pressures (P1 – P2) (Figure 1.8), ranging from 9.3 to 11.4 mmHg in healthy humans (Piñero et al., 2014).

b) Corneal Resistance Factor (CRF) is derived from the two applanation pressures taking into account the CCT. It represents the resistance of the cornea and could be calculated by equation: CRF = (P1 − 0.7 x P2) (Luce, 2005).

c) The Goldmann-correlated IOP (IOPg) is calibrated to match the Goldmann applanation tonometry as closely as possible by the average of P1 and P2.

d) Corneal-compensated IOP (IOPcc) is obtained by the equation IOPcc = P1 − 0.43 x P2. This IOP value is less influenced by CCT (Luce, 2005).

As stated in the previous studies, a reliable ORA measurement refers to two applanation signal peaks with approximately symmetrical height and a waveform with a relatively smooth signal curve. A waveform score in a range of 0 to 10 is provided to indicate measurement quality. There is no guideline for the use of waveform scores from the manufacturer. The quality of ORA measurements is better with a higher waveform score. Previous studies recommended a waveform score of at least 3.6 and averaging three measurements to increase measurement reliability (Lam et al., 2010; Mandalos et al., 2013; Vantomme et al., 2013).

2.1.4 Statistical analysis

Statistical analysis and graphics were performed using SPSS (version 26.0, IBM, Armonk, NY., USA) and Origin (Version 9.85.204, OriginLab, Inc., USA) software, respectively. All the data were tested for normality using Shapiro-Wilk tests. Appropriate parametric or nonparametric statistical tests were used for analysis. The level of significance was set at 5%.

A test-retest repeatability (TRR) of IOP was first calculated from the baseline of the IOP before the ocular compression. The TRR was the within-subject standard deviation (Sw) × √2*1.96, where Sw was derived from three baseline IOP readings obtained within one minute (Bland et al., 1996). Then “Baseline IOP” and “Compression IOP” were calculated, as the average of three IOP readings before the ocular compression and the average of all IOP readings obtained during ocular compression, respectively. Subjects with “Immediate IOP Rise” (IOP at compression time-zero minus Baseline IOP) smaller than the TRR were excluded.

The average and standard deviation of demographic characteristics were calculated. Mann-Whitney test and independent t-test were performed to compare the two myopic groups. Since AL and SER had positively skewed distributions (Chen et al., 2016), the Mann-Whitney test was applied for these two parameters. Linear regression analysis

was applied to determine the IOP decline rate during the ocular compression in each group. Two-tailed independent t-test was used to study the difference in the decline slopes of the two groups. For pairwise comparisons, repeated-measures analysis of variance (RMANOVA) and Friedman test with Bonferroni correction post hoc tests were used to determine the time point when IOP returned to baseline level by comparing Baseline IOP and IOP readings during the recovery phase.

2.2 Results

In the pilot study, the TRR was 2.6 mmHg, and no subject was excluded. Table 2.1 shows the clinical demographics of all subjects (n = 34). IOP from all subjects showed a decreasing trend during the ocular compression (Figure 2.6). Immediately after ocular compression (R-0S), IOP was lower than the baseline IOP of 14.3 mmHg. Afterward, the IOP slowly returned to the baseline IOP during the recovery phase.

Table 2.1 Demographic characters of all subjects (n = 34) in the pilot study. Data are presented as mean ± standard deviation.

Parameters	**Mean ± SD**
Age (years)	25.2 ± 2.5
AL (mm)	25.4 ± 1.2
SER (D)	-5.21 ± 3.18
Baseline IOP (mmHg)	14.3 ± 3.3
Immediate IOP Rise (mmHg)	14.3 ± 6.8
Compression IOP (mmHg)	26.5 ± 6.0

AL: axial length; SER: spherical equivalent refractive error; D: diopter; IOP: intraocular pressure; Baseline IOP: the average of three IOP readings within 1 min before ocular compression; Immediate IOP Rise: IOP at compression time-zero minus Baseline IOP; Compression IOP: the average of all IOP readings obtained during ocular compression within 1 min.

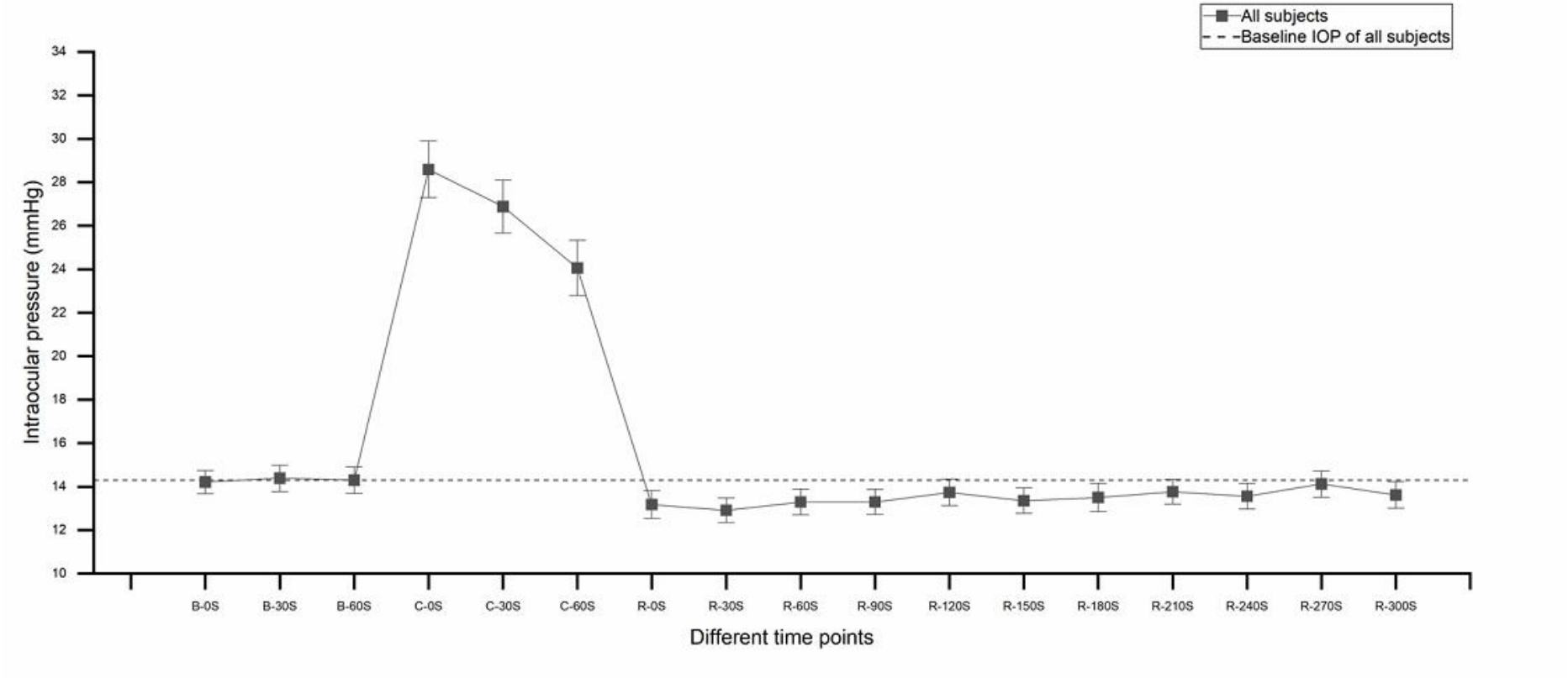

Figure 2.6. IOP of all 34 subjects before, during, and after the ocular compression in the pilot study. B: Baseline; C: Compression; R: Recovery. The data were plotted as mean ± standard error. Black dotted line: Baseline IOP of 14.3 mmHg.

In the extended study, the TRR was 2.4 mmHg, and all the 60 subjects (30 HM vs 30 LM) were included for analysis. Refer to Table 2.2, both LM and HM groups had similar age (p = 0.153), Baseline IOP (p = 0.988), Immediate IOP Rise (p = 0.960), as well as the Compression IOP (p = 0.877). Although the two groups had similar IOPg (p = 0.454), the HM group had higher IOPcc than the LM group (16.3 ± 2.4 mmHg vs 14.5 ± 2.8 mmHg, independent t-test, p = 0.009). The LM group also had higher CH than HM (10.8 ± 1.6 mmHg vs 9.6 ± 1.4 mmHg, independent t-test, p = 0.002) and higher CRF than HM (10.4 ± 1.6 mmHg vs 9.5 ± 1.6 mmHg, independent t-test, p = 0.037).

Figure 2.7 shows the IOP change of LM (n = 30) and HM (n = 30) before, during, and after the ocular compression. The coefficients of determination (R^2) of the regression lines (i.e., IOP decline rate in HM and LM during the ocular compression) were 0.98 and 0.99, respectively. HM had a slower IOP decline rate of -2.58 mmHg/min (95% confidence interval (CI), -3.24 ~ -1.98 mmHg/min) than LM, -3.24 mmHg/min (95%CI, -3.84 ~ -2.64 mmHg/min). The difference in the decline rates was not significant (p = 0.0528).

Pairwise comparisons using RMANOVA for HM and Friedman test for LM were performed to compare IOP readings from R-0S to R-600S with the Baseline IOP. In HM, IOP in R-450S, and from R-510S to R-600S were not significantly different from the Baseline IOP. In LM, IOP from R-240S to R-300S, and from R-360S to R-600S were similar to the Baseline IOP. This indicated that IOP of LM returned to its baseline level faster than HM did.

Table 2.2 Demographic characteristics and comparison results of study subjects (n = 60, 30 HM vs 30 LM) in extended study. Data are presented as mean ± standard deviation.

Parameters	All subjects	HM group	LM group	P Value″
Age (years)	23.9 ± 2.8	24.3 ± 2.7	23.4 ± 3.0	0.153*
AL (mm)	25.5 ± 1.5	26.6 ± 1.1	24.4 ± 0.9	< 0.001*
SER (D)	-4.81 ± 3.30	-7.89 ± 1.39	-1.74 ± 0.82	< 0.001*
Baseline IOP (mmHg)	14.9 ± 2.8	14.9 ± 2.8	14.9 ± 2.8	0.988†
Immediate IOP Rise (mmHg)	10.3 ± 4.3	10.2 ± 3.9	10.3 ± 4.7	0.960†
Compression IOP (mmHg)	22.0 ± 4.0	22.3 ± 4.2	21.7 ± 3.8	0.877*
IOPcc (mmHg)	15.4 ± 2.7	16.3 ± 2.4	14.5 ± 2.8	0.009†
IOPg (mmHg)	14.5 ± 2.7	14.8 ± 2.8	14.3 ± 2.7	0.454†
CH (mmHg)	10.2 ± 1.6	9.6 ± 1.4	10.8 ± 1.6	0.002†
CRF (mmHg)	10.0 ± 1.7	9.5 ± 1.6	10.4 ± 1.6	0.037†

AL: axial length; SER: spherical equivalent refractive error; D: diopter; IOP: intraocular pressure; Baseline IOP: the average of three IOP readings within 1 min before ocular compression; Immediate IOP Rise: the difference between IOP at compression time-zero and Baseline IOP; Compression IOP: the average of all IOP readings obtained during ocular compression within 2 min; IOPcc: corneal-compensated IOP; IOPg: Goldmann-correlated IOP CH: corneal hysteresis; CRF: corneal resistance factor.

″The comparison between HM and LM group; *Mann-Whitney test; †Independent t-test.

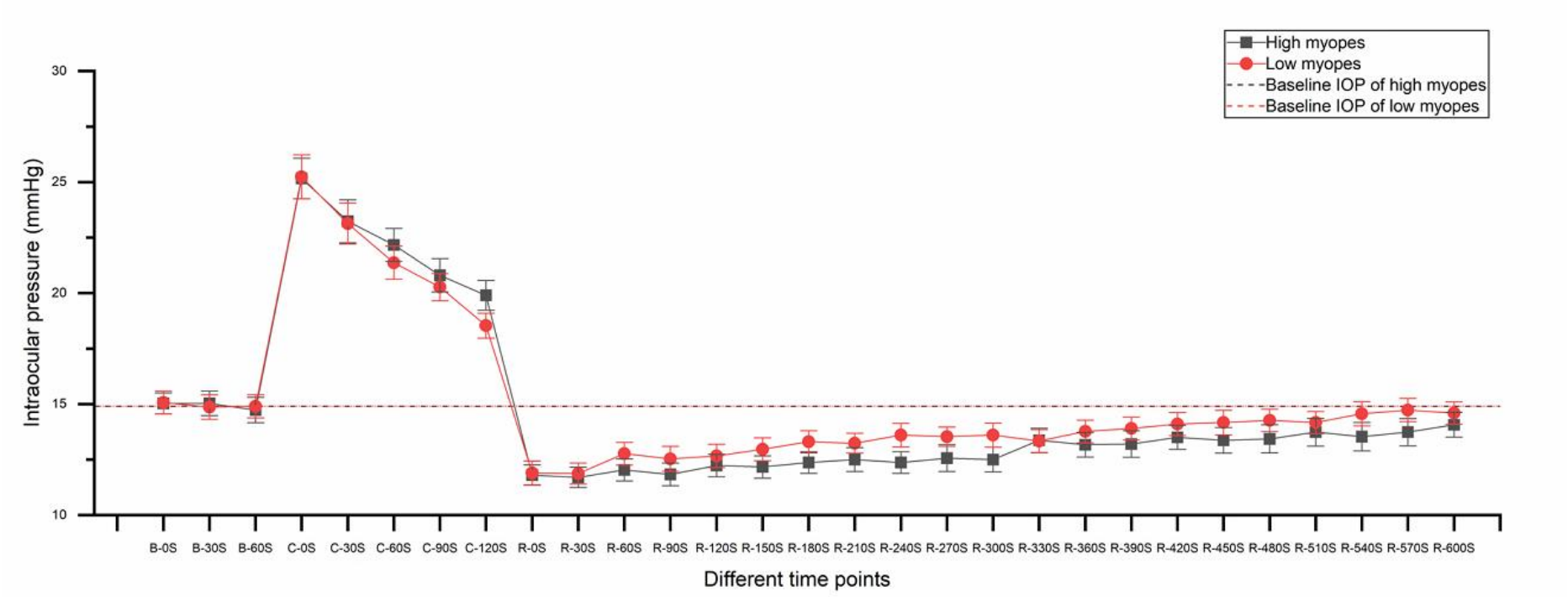

Figure 2.7. IOP of high myopes (n = 30) and low myopes (n = 30) before, during, and after the ocular compression. B: Baseline; C: Compression; R: Recovery. The data were plotted as mean ± standard error. The red solid line: average IOP values of low myopes in specific time points. Black solid line: average IOP values of high myopes in specific time points. The black dotted line: Baseline IOP of high myopes of 14.9 mmHg; Red dotted line: Baseline IOP of low myopes of 14.9 mmHg.

2.3 Discussion

This study indicated that IOP was not constant, but it gradually dropped during the ocular compression. Previous studies were incorrect to assume a constant IOP during OCT scans (Zhang et al., 2020). After release of the compressive force, IOP was lower than the baseline IOP and slowly returned to the baseline level slowly. The two refractive groups performed differently during and after IOP elevation.

Since IOP kept on changing during and after the ocular compression, this could be related to aqueous humor outflow. The aqueous humor flows into the Schlemm's canal through the trabecular meshwork and finally returns to the episcleral vessels to maintain a relatively constant IOP level. The cells of trabecular meshwork and Schlemm's canal can adjust the aqueous outflow to control the IOP (Abu-Hassan et al., 2015; Acott et al., 2014). The IOP homeostatic mechanism theory proposed that IOP could be maintained due to the adjustment of the pulsatile aqueous humor outflow (Johnstone, 2014). This theory also mentioned that when IOP was reduced below its physiologic set point, the pulsatile aqueous flow would stop, but resume when IOP is raised to the homeostatic set point. It is possible that such a high IOP increase (average rise of 14 mmHg in the pilot study and 10 mmHg in the extended study) may exceed the safety limit. Correspondingly, outflow resistance shifted its levels to reduce the IOP to an acceptable level during IOP elevation. After the external force was removed, aqueous humor outflow resistance adjusted to facilitate the return of the IOP back to its pre-elevated level. Thus, aqueous humor dynamics may explain the IOP changes in this study.

During the course of the current study, Chen et al. (2020) reported their findings of Schlemm's canal dimensions during ophthalmodynamometry. They applied SD-OCT to monitor the Schlemm's canal when increasing IOP for 4 minutes. IOP demonstrated a decay in an exponential manner. The Schlemm's canal collapsed immediately after the ocular compression when IOP was at its highest. The cross-sectional area of

Schlemm's canal gradually increased during ocular compression with the IOP slowly reducing. Their study supported the theory that the change of IOP is related to aqueous outflow facility regulated through different dimensions of the Schlemm's canal. However, they did not measure the change of the IOP after the ocular compression. Therefore, how IOP would return to the baseline level and Schlemm's canal dimensions would change, is still unclear.

Similarly, Iwase et al. (2018) reported a slight decline in IOP during ocular compression. They increased IOP for 10 minutes using an ophthalmodynamometer and monitored IOP regularly using rebound tonometry. After releasing the external pressure, the IOP returned to baseline level with a tiny drop. The detailed mechanism has not been determined yet.

Previous studies have compared the morphological changes of the LC before and during ocular compression (Beotra et al., 2018; Tun et al., 2016; Zhang et al., 2020). Since imaging the ONH with SD-OCT took around 2 minutes, IOP during ocular compression was measured only once before the imaging, which could not represent the true IOP level during ONH imaging. Hence, it is more likely that IOP was lower than the expected level during ONH imaging. Their derived LC indices could be under-estimating the true LC responses. To rectify the problem, researchers could perform tonometry before and after imaging the ONH. Assuming a steady decline of IOP during the ocular compression, an average of these two IOP values may represent the IOP level during ONH imaging.

Results from the pilot study initiated the extended study to compare the IOP dynamics of the two myopic groups. Although IOP decline rates differed between the two groups, they did not reach statistical significance (p = 0.0528). However, the IOP of LM returned to the baseline level faster. This may be due to the differences in aqueous humor outflow facilities between the two groups. Aqueous outflow facility is not a

routine ophthalmic procedure. Neither fluorophotometry (Fernández-Barrientos et al., 2010; Guo et al., 2017) nor manometric methods (Karyotakis et al., 2015) are feasible to be applied in clinical practice. Perhaps monitoring IOP changes through ocular compression could be an alternative way to study aqueous humor dynamics.

Morphologically, it is hypothesized that weak IOP adjustment ability may be due to the different structures in Schlemm's canal and trabecular meshwork in HM (Chen et al., 2018; Qi et al., 2020). HM had lower CH and CRF than LM (Table 2.3). Lower CH and CRF have been previously reported in glaucoma (Gatzioufas et al., 2013; Pillunat et al., 2016). High myopia is a risk factor for glaucoma and high myopes usually have higher baseline IOP than low myopes (Quinn et al., 1995). It is possible high myopes may have a weaker ability to regulate IOP due to poor aqueous outflow facility when IOP level exceeds an acceptable level. The outflow facility may be influenced by the biomechanics of the Schlemm's canal and trabecular meshwork. How aqueous outflow facility is related to ocular biomechanics requires further studies.

This study has several limitations. First, in the pilot study, subjects performed ocular compression by themselves. Some subjects could not steadily hold the Proview™. In the extended study, a mounting device was used to fix the Proview™. The Immediate IOP was obtained around 15 to 20 seconds after the commencement of the ocular compression by the Proview™. This could explain why the Immediate IOP Rise was lower in the extended study (10.3 ± 4.3 mmHg) than in the pilot study (14.3 ± 6.8 mmHg). Second, muscle and fatty tissues beneath the lower eyelid differed among subjects. The force transmitted to the eyeball could be different even after the same compressive force is applied. However, as the Immediate IOP Rise and Compression IOP were similar between HM and LM, this factor should not significantly influence the results. Third, the current study only included young adults. These findings might not apply to older adults who are more prone to glaucoma. Finally, the anterior

segment was not measured, such as the use of SD-OCT, as performed by Chen et al. (2020).

To conclude, IOP was not stable during the ocular compression, but showed a steady decline. High and low myopes demonstrated different IOP profiles during and after the ocular compression. Since it could be difficult to image ONH and monitor IOP simultaneously, ocular compression was not applied in the following study when evaluating the LC shape.

3. Study 2: Association between corneal biomechanics and lamina cribrosa shape

In Study 1, given that ONH is difficult to image while monitoring the IOP simultaneously, and the mechanism of IOP dynamic during ocular compression remains unclear, ocular compression was not applied in Study 2 when evaluating the LC shape. Instead of applying the parameters of LC change by ocular compression, some static parameters about LC morphology would be used to indicate LC biomechanical properties. Previous studies proposed that LCCI could reflect the strain of ONH (Kim et al., 2020). Hence, LCCI was applied in Study 2.

3.1 Methodology

3.1.1 Subjects

G*Power (version 3.1.9.6) was performed to determine the appropriate sample size, to detect a significant difference in corneal hysteresis (Jiang et al., 2011) and corneal tangent modulus (Hon et al., 2017) between low and high myopes with the one-tailed α of 0.05 and statistical power of 90%. G-power showed that at least 31 subjects in each group should be required.

Healthy young adults of different myopia status were recruited within the university campus. The study protocol was approved by the Human Subjects Ethics Committee of The Hong Kong Polytechnic University and adhered to the tenets of the Declaration of Helsinki. Written voluntary informed consent was obtained from each subject prior to any eye measurements.

Inclusion criteria of the subjects were as follows:

a. Chinese aged between 20 to 30 years
b. No history of ocular disease, trauma, or surgery
c. Currently not taking any medication

d. Low myopes (-3.00D ≤ SER ≤ -0.50D) in both eyes, or high myopes (SER ≤ -6.00D) in both eyes
e. Best corrected visual acuity of at least LogMAR 0.00 in each eye

Exclusion criteria were listed as follows:

a. IOPcc or IOPg > 21 mmHg
b. Waveform score < 3.6 from ORA
c. Contact lens wearing

3.1.2 Measurement of corneal tangent modulus

As an elastic parameter, Young's modulus can describe the relationship between stress and strain but cannot indicate the viscoelastic properties of the cornea. Therefore, corneal tangent modulus was proposed to describe the elastic behaviors of the cornea (Buzard, 1992; Ko et al., 2013; Lam et al., 2015). Together with the measurement of corneal hysteresis, this allows viscoelastic properties to also be investigated.

The corneal indentation device (CID) (Figure 3.1) was developed to measure the corneal tangent modulus (Ko et al., 2013). The CID could measure the force required to displace the cornea to one mm depth using a small indenter. The corneal tangent modulus can be calculated with the information from CCT and corneal radius after determining the corneal stiffness from each acquisition (displayed on the CID screen) (Hon et al., 2017).

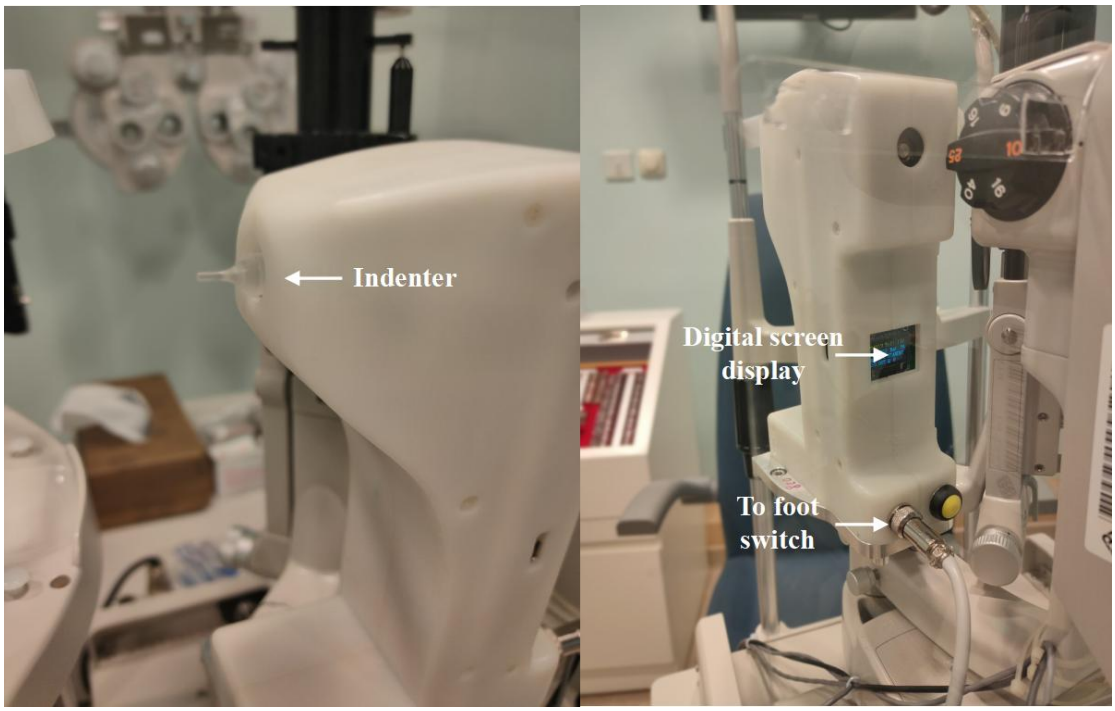

Figure 3.1. The corneal indentation device. The CID was mounted on a slit-lamp base.

3.1.3 Measurement of the lamina cribrosa

The Spectralis (Heidelberg, Germany), is a commonly used SD-OCT device that can capture a deeper structure of the ONH through an Enhanced Depth Imaging (EDI) function (Lee et al., 2011). Its eye tracking function can further enhance the precise location of the ONH. Since blood vessels at the ONH could block the visibility of the LC, an adaptive compensation function was applied to enhance the identification of the anterior LC surface (Figures 3.2A and 3.2B) (Girard et al., 2011; Mari et al., 2013).

The anterior LC surface was initially sketched to derive the LCCI. A perpendicular line was drawn from each BMO to reach the anterior LC surface. The length of the line connecting the two ends of the anterior LC was the width (*W*). The greatest distance from this new line to the anterior LC surface was the LC curve depth (LCCD) (Figure 3.2C). LCCI was calculated as (LCCD/*W*) × 100 (Kim et al., 2020; Lee et al., 2019). In the example shown in Figure 3.2C, the *W* length on the anterior LC surface

and LCCD was 1475.32 µm and 109.74 µm, respectively. LCCI value was (109.74/1475.32) *100 = 7.438. The middle LCD was the distance from the middle of a reference line joining the two BMO to the anterior LC surface. The maximum LCD was the greatest distance from the BMO reference line to the anterior LC surface (Figure 3.2D).

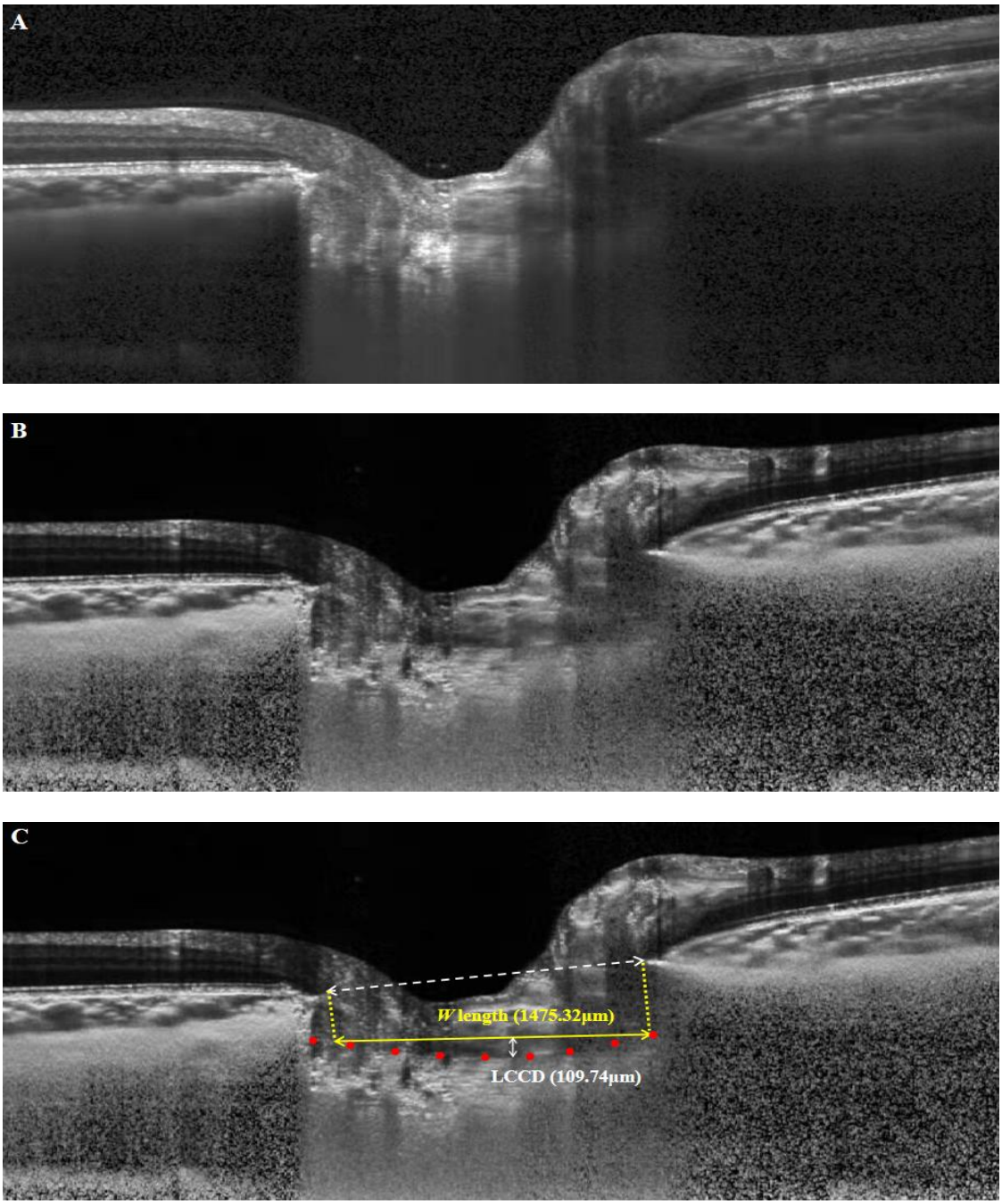

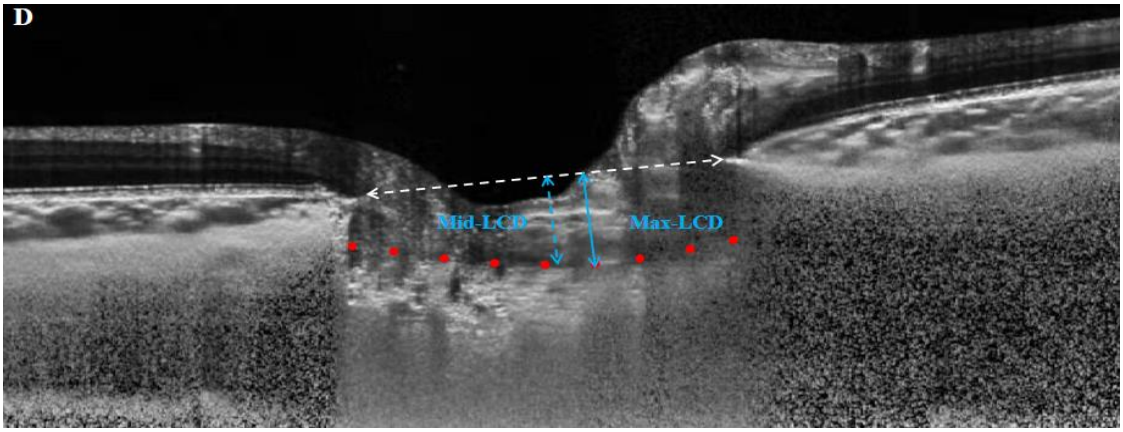

Figure 3.2. The measurement of the LCCI and LCD. (A) Original B-scan image of the ONH **(B)** Same B-scan image in **A** after processing by adaptive compensation. **(C)** The LCCI was calculated by multiplying the ratio of the LCCD (white double-headed dashed line) and the length of the anterior LC surface reference line (*W*, yellow double-headed line) by 100. **(D)** Max-LCD (blue solid line) is the maximum depth from the BMO reference line (white dashed line) to the anterior LC surface (red dots); Mid-LCD (blue dashed line) is the depth from the middle of the BMO reference line to anterior LC surface.

3.1.4 Procedures

Of the 176 healthy subjects initially recruited, only 32 LM and 32 HM completed the study. The following measurements were obtained from all subjects: AL, corneal curvature, and CCT measured using AL-Scan^{TM} (Nidek Co., Ltd, Japan); fundus photos captured by a non-mydriatic retinal camera (TRC-NW8. Topcon, Japan); automated objective refraction (ARK-510A, Nidek Co., Ltd., Japan) followed by subjective refraction; RNFL thickness measurement using the Cirrus HD-OCT (Carl Zeiss Meditec, Inc., CA) with the signal strength score of at least 7; LC was imaged using the EDI function of SD-OCT (Spectralis, Heidelberg, Germany). Before scanning, the mean corneal radius of each eye was entered into the Spectralis SD-OCT based on the manufacturer's instructions to reduce measurement bias. The image quality of all scans was higher than 20.0. The visibility of the LC was enhanced by applying the adaptive compensation function with a manual caliper tool in the

Reflectivity (Version 1.0.0). A readable LC anterior surface was obtained for 64 subjects. Three readings (waveform score ≥ 3.6) of corneal biomechanical parameters (IOPcc, IOPg, CH, CRF) were recorded using the ORA (Reichert Inc., Depew, New York, USA) (Lam et al., 2010). The final measurement was the tangent modulus using the CID because of the use of topical anesthesia. All measurements were completed between 10:00 am and 2:00 pm to reduce diurnal variation of different ocular parameters.

The Spectralis SD-OCT device was set to image a 15° × 10° rectangle centered on the ONH under high-resolution scanning (768 A-scan per B-scan), and high-speed mode (384 A-scan per B-scan). This rectangle scanning included 97 section B-scan images with a distance of 30–35μm from each other. In each section, 42 OCT frames were averaged.

The LCCI and LCD of each eye were determined from three selected horizontal OCT B-scan images, equidistant across the vertical optic disc diameter. Previous studies that apply LCCI divided the vertical optic disc diameter into seven equidistant horizontal planes, which was similarly performed in the current study. However, only three horizontal OCT B-scans were used, namely the superior mid-periphery, mid-horizontal, and inferior mid-periphery (Figure 3.3), because more planes could alleviate the assessment of LC bowing (Lee et al., 2018). The corresponding LCCI from these three planes were named LCCI_sup, LCCI_mid, and LCCI_inf, respectively. LCCI measurement was performed by an experienced examiner, who was masked to the subjects' information. One eye from each subject was randomly selected for statistical analyses unless only one eye was available because of the difficulty in identifying the LC anterior surface.

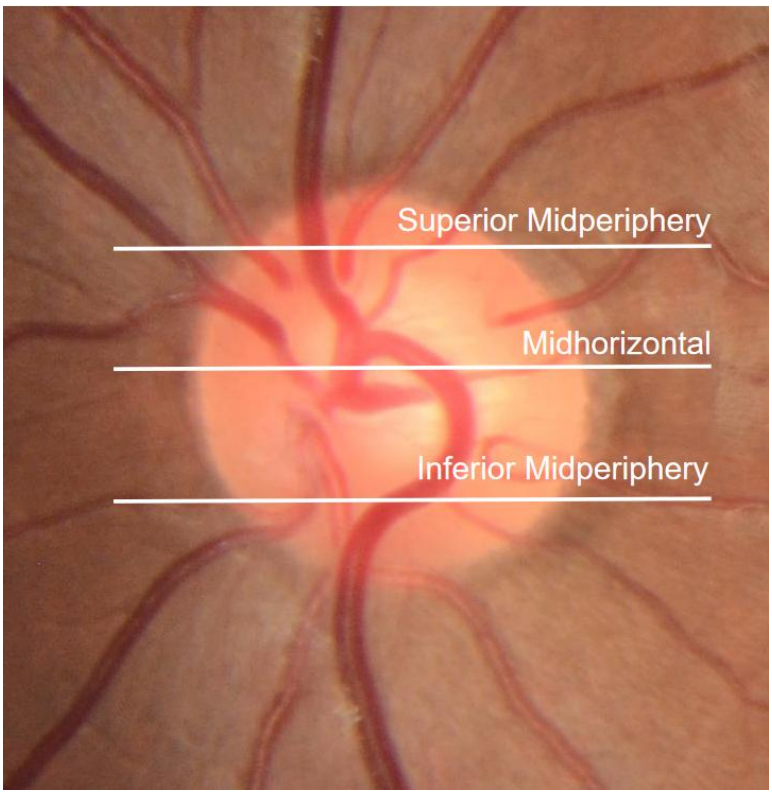

Figure 3.3. Optic disc photographic image with three lines spaced with the same distance across the vertical optic disc diameter. Three selected B-scan images were located equidistant across the vertical optic disc diameter.

Before measuring the CID, each subject was prepared using a drop of 0.5% proparacaine for topical anesthesia. The subject was required to keep a stable and external fixation target with their chin on the chinrest. When the 2-mm diameter probe was properly aligned and touched the central corneal surface, a beep sound was then provided. After pressing the foot switch, the probe indented the cornea at a depth of 1 mm, and subsequently, retracted at a speed of 12 mm/second. One acquisition took around 0.2 seconds. After each measurement, the corresponding corneal stiffness representing the slope of the force-displacement curve was immediately displayed on the screen. The calculated tangent modulus was normalized to 15.5 mmHg (the mean IOP of normal eyes (King et al., 2013)) using IOPcc because the tangent modulus is IOP-dependent (Hon et al., 2017).

3.1.5 Statistical analysis

Statistical analysis and graphics were conducted using the SPSS (version 26.0, IBM, Inc., Armonk, NY, USA) and Origin (Version 9.85.204, OriginLab, Inc., USA) software, respectively. The distributions of the data sets were tested for normality using the Shapiro-Wilk tests. Appropriate parametric or nonparametric statistical tests were applied. The level of significance chosen was set at 5%.

A total of 68 horizontal OCT images were selected and evaluated by another masked experienced examiner to determine the interobserver reproducibility of LCCI measurement. The ICC and the 95% Bland-Altman limits of agreement between two examiners were calculated. Independent t-test and Mann-Whitney test were used based on the normality of the data. Pearson's chi-squared test was used to compare the gender distribution of the two groups. Wilcoxon signed rank test was applied to compare the Mid-LCD and Max-LCD in each group. LCCI values among the three planes of each refractive group were analyzed by repeated-measures analyses of variance (RMANOVA). Average LCCI of each eye was calculated using the three planes' LCCI values and used for further analysis. Univariate analysis was conducted to assess the associations of Average LCCI (as a dependent variable) and AL, CCT, CH, CRF, IOPcc, corneal tangent modulus (E_N), and RNFL thickness (as independent variables). Whenever significant correlation was found, those ocular parameters were included in the multivariate regression analysis.

3.2 Results

From the flowchart (Figure 3.4), there were a total of 176 subjects who originally participated, and most of them were excluded because of the unsuccessful CID measurement and poor image quality of the LC. Only data of 32 LM and 32 HM were available.

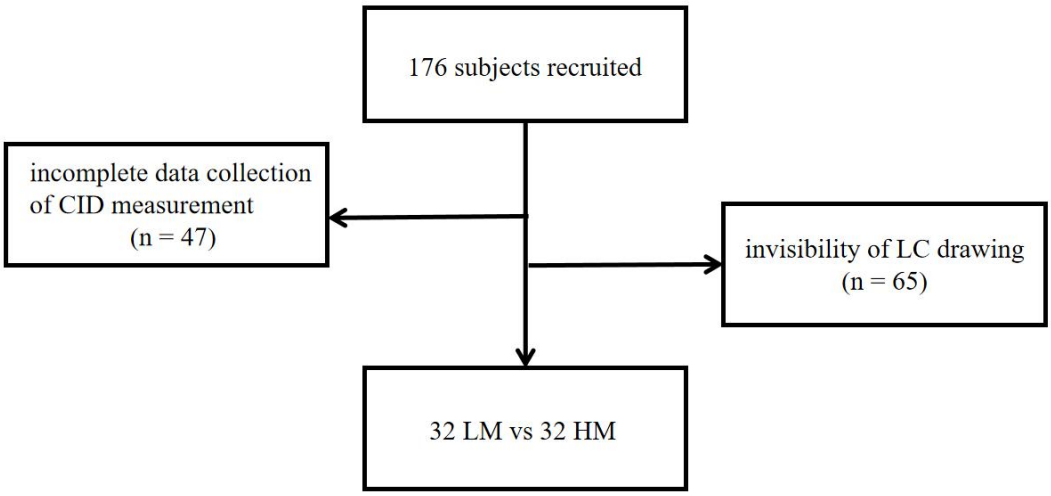

Figure 3.4. Flowchart of subject screening.

There was excellent interobserver reproducibility in LCCI measurement (ICC = 0.968, 95% CI = 0.949–0.991, two-way mixed-effect model, absolute agreement). The mean difference in LCCI was 0.115, with 95% limits of agreement ranging from 1.211 to -0.980 (Figure 3.5).

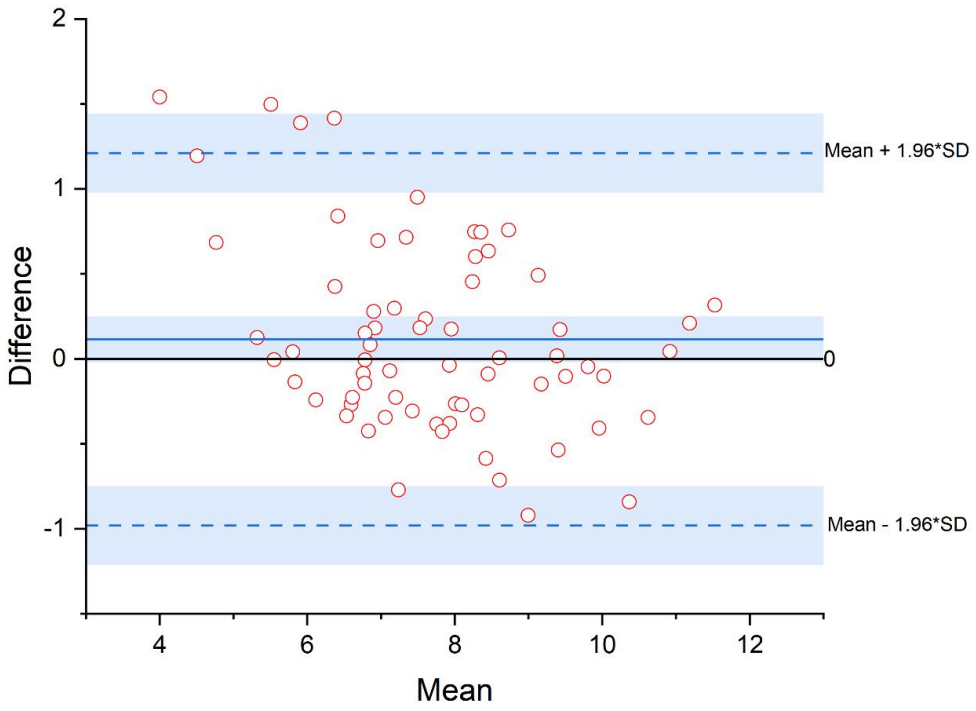

Figure 3.5. The 95% Bland-Altman limits of the agreement showing the reproducibility of LCCI. The upper and lower blue dotted lines indicate the upper and lower limits of agreement (Mean ± 1.96*SD), respectively. The blue solid line represents the mean difference.

Table 3.1 shows the demographic characteristic of all subjects and the comparison between HM and LM. Considering the inclusion criteria, LM and HM showed significant differences in SER ($p < 0.001$) and AL ($p < 0.001$). Since axial elongation is the main cause of myopia development (Hou et al., 2018), only AL was used for further analysis. There were no significant differences found in gender distribution between the two groups ($p = 0.062$). The two myopic groups had similar CCT ($p = 0.068$), RNFL thickness ($p = 0.160$), and CRF ($p = 0.358$). In addition, HM had significantly higher IOPcc ($p < 0.001$), higher IOPg ($p = 0.027$), and lower CH ($p = 0.012$) than LM. In addition, HM had lower significantly corneal stiffness ($p = 0.001$) and corneal tangent modulus ($p < 0.001$) than LM.

Table 3.1 Demographic characteristics and comparison results of study subjects (n = 64, 32 HM vs 32 LM). Data are presented as mean ± standard deviation.

Parameters	All subjects	HM group	LM group	P Value″
Age (years)	24.17 ± 3.08	23.78 ± 2.81	24.17 ± 3.08	0.314†
AL (mm)	25.27 ± 1.53	26.40 ± 1.18	24.14 ± 0.84	< 0.001*
SER (D)	-5.068 ± 3.51	-8.250 ± 1.892	-1.887 ± 0.762	< 0.001*
Female/Male	43/21	25/7	18/14	0.062‡
CCT (μm)	557.08 ± 31.18	549.97 ± 31.12	564.19 ± 30.05	0.068†
RNFL thickness (μm)	97.44 ± 8.69	95.91 ± 7.74	98.97 ± 9.42	0.160†
IOPcc (mmHg)	15.65 ± 2.35	16.76 ± 1.95	14.55 ± 2.22	< 0.001†
IOPg (mmHg)	14.59 ± 2.51	15.28 ± 2.60	13.91 ± 2.25	0.027†
CH (mmHg)	9.99 ± 1.47	9.53 ± 1.30	10.45 ± 1.50	0.012†
CRF (mmHg)	9.80 ± 1.60	9.61 ± 1.65	9.98 ± 1.56	0.358†
Stiffness (N/mm)	0.063 ± 0.054	0.061 ± 0.005	0.065 ± 0.005	0.001†
E_N (MPa)	0.476 ± 0.093	0.434 ± 0.070	0.518 ± 0.095	< 0.001†

AL: axial length; SER: spherical equivalent refractive error; D: diopter; CCT: central corneal thickness; RNFL: retinal nerve fiber layer; IOPcc: corneal-compensated intraocular pressure; IOPg: Goldmann-correlated intraocular pressure; CH: corneal hysteresis; CRF: corneal resistance factor; E_N: normalized corneal tangent modulus.
″Comparison between HM and LM group; *Mann-Whitney test; †Independent t-test; ‡Pearson's chi-squared test.

As shown in Table 3.2, LM had a higher Average LCCI ($p < 0.001$) and higher LCCI values at all three planes ($p \leq 0.05$) than HM. Mid-LCD and Max-LCD were significantly different between groups (Wilcoxon signed rank test, $p < 0.001$). Although LM had larger Mid-LCD than HM at all the three planes, Max-LCD values were not significantly different between the two groups. Figure 3.6 shows LCCI of the subjects in three different regions. The LCCI values at different planes were similar in HM ($p > 0.05$), whereas the LCCI at the superior plane was higher than the mid-horizontal plane in LM ($p = 0.007$).

Table 3.2 LCCIs, Mid-LCD, and Max-LCD in different planes. Data are represented as mean ± standard deviation.

LCCIs	All subjects	HM group	LM group	P value″
LCCI_sup	7.50 ± 2.09	6.42 ± 1.55	8.58 ± 2.02	< 0.001†
LCCI_mid	6.70 ± 1.78	6.10 ± 1.51	7.30 ± 1.84	0.005*
LCCI_inf	7.13 ± 1.80	6.61 ± 1.25	7.64 ± 2.12	0.022†
Average LCCI	7.11 ± 1.50	6.37 ± 1.05	7.84 ± 1.54	< 0.001†
Mid_LCD_sup (μm)	388.72 ± 95.30	356.64 ± 87.79	420.80 ± 92.87	0.003*
Max_LCD_sup (μm)	449.28 ± 97.77	440.98 ± 91.62	457.59 ± 104.36	0.413*
Mid_LCD_mid (μm)	370.62 ± 95.70	342.00 ± 88.66	399.25 ± 95.18	0.005*
Max_LCD_mid (μm)	426.91 ± 101.62	426.50 ± 93.96	427.32 ± 110.26	0.914*
Mid_LCD_inf (μm)	352.11 ± 91.44	326.51 ± 96.70	377.71 ± 90.14	0.009*
Max_LCD_inf (μm)	411.79 ± 92.37	408.55 ± 85.78	415.03 ± 99.80	0.799*
Mid-LCD (μm)	370.48 ± 91.06	341.71 ± 83.93	399.25 ± 90.00	0.005*
Max-LCD (μm)	429.33 ± 93.46	425.34 ± 86.54	433.31 ± 101.13	0.687*

LCCI_sup: LCCI in superior mid-periphery plane; LCCI_mid: LCCI in mid-horizontal plane; LCCI_inf: LCCI in inferior mid-periphery plane; Average LCCI: mean of LCCI in all three planes; Mid_LCD_sup: LC depth from anterior LC surface to middle BMO level in superior mid-periphery plane; Mid_LCD_mid: LC depth from anterior LC surface to middle BMO level in mid-horizontal plane; Mid_LCD_inf: LC depth from anterior LC surface to middle BMO level in inferior mid-periphery plane; Max_LCD_sup: maximum depth from anterior LC surface to BMO level in superior mid-periphery plane; Max_LCD_mid: maximum depth from anterior LC surface to BMO level in mid-horizontal plane; Max_LCD_inf: maximum depth from anterior LC surface to BMO level in inferior mid-periphery plane; Mid-LCD: mean of Mid_LCD in all three planes; Max-LCD: mean of Max_LCD in all three planes.
″Comparison between HM and LM group; *Mann-Whitney test; †Independent t-test

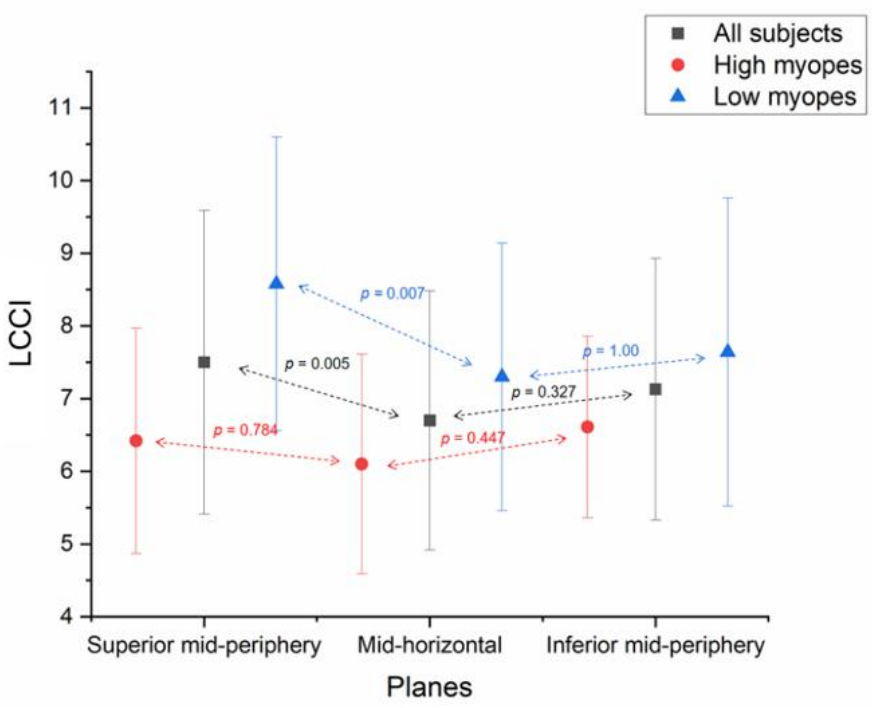

Figure 3.6. LCCIs in three different regions. All subjects and high myopes had similar LCCIs in the three planes; LCCI in the superior plane was higher than the mid-horizontal plane in low myopes. *P* values were a comparison of the LCCI between adjacent planes. The data was plotted as mean ± standard deviation.

Table 3.3 shows the regression analysis of the Average LCCI and different ocular parameters. Average LCCI was significantly correlated with AL ($p < 0.001$, Figure 3.7), CH (r = 0.248, $p = 0.048$, Figure 3.8), IOPcc (r = -0.259, $p = 0.039$, Figure 3.9), and RNFL thickness (r = 0.307, $p = 0.014$, Figure 3.10) in univariate analysis. However, there was no significant association between the Average LCCI and the corneal tangent modulus (r = 0.136, $p = 0.286$). Multivariate analysis shows that Average LCCI was only significantly associated with AL (r = -0.378, $p = 0.003$).

Table 3.3 Multiple regression of factors associated with Average LCCI from all subjects (n = 64).

	Univariate Analysis		Multivariate Analysis	
Parameters	**Standardized**	**P value**	**Partial**	**P value**
AL (mm)	-0.533	< 0.001	-0.378	0.003
CCT (μm)	0.205	0.103	-	-
CH (mmHg)	0.248	0.048	0.139	0.286
CRF (mmHg)	0.143	0.261	-	-
IOPcc (mmHg)	-0.259	0.039	0.001	0.996
E_N (MPa)	0.136	0.286	-	-
RNFL thickness (μm)	0.307	0.014	0.151	0.186

AL: axial length; CCT: central corneal thickness; CH: corneal hysteresis; CRF: corneal resistance factor; IOPcc: corneal-compensated IOP; E_N: normalized corneal tangent modulus; RNFL: retinal nerve fiber layer.

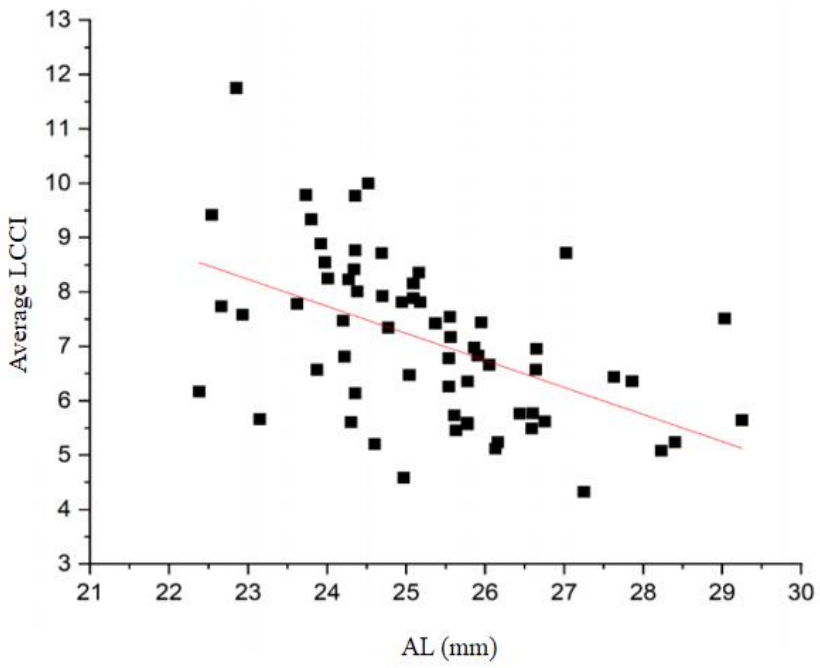

Figure 3.7. Scatter plot showing that AL had a negative association with the Average LCCI. Pearson correlation coefficient (r) = -0.533, $p < 0.001$.

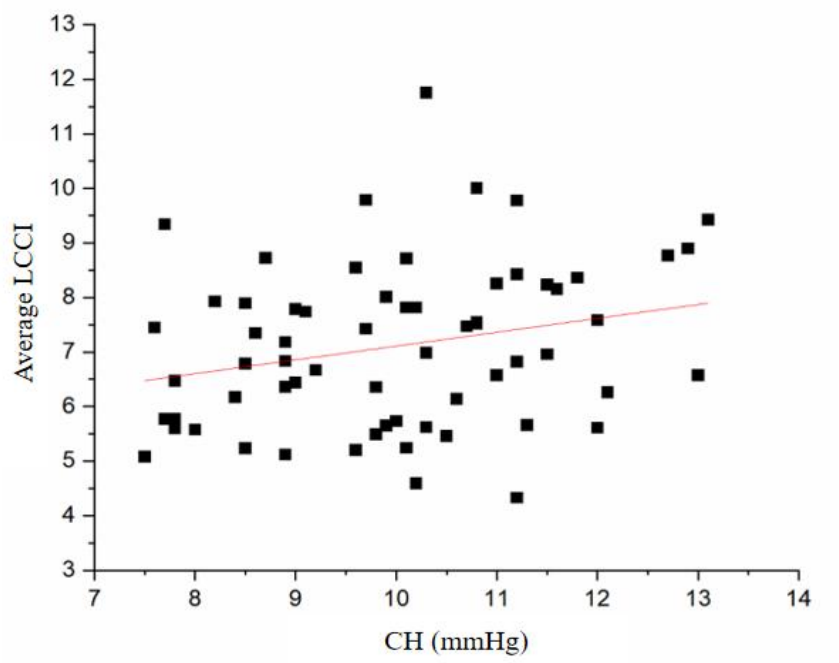

Figure 3.8. Scatter plot showing that the CH had a positive association with the Average LCCI. Pearson correlation coefficient (r) = 0.248, $p = 0.048$.

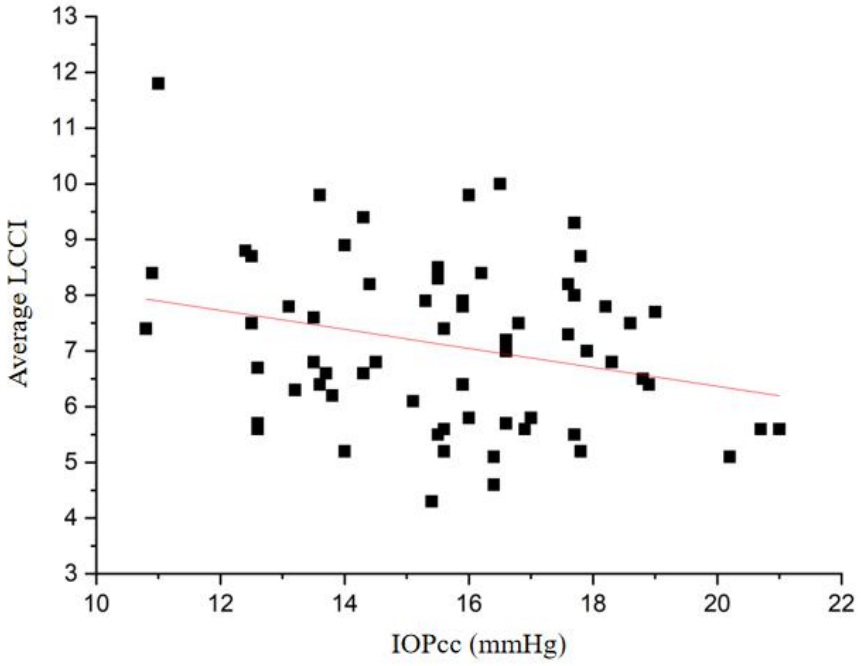

Figure 3.9. Scatter plot showing that IOPcc had a negative association with the Average LCCI. Pearson correlation coefficient (r) = -0.259, p = 0.039.

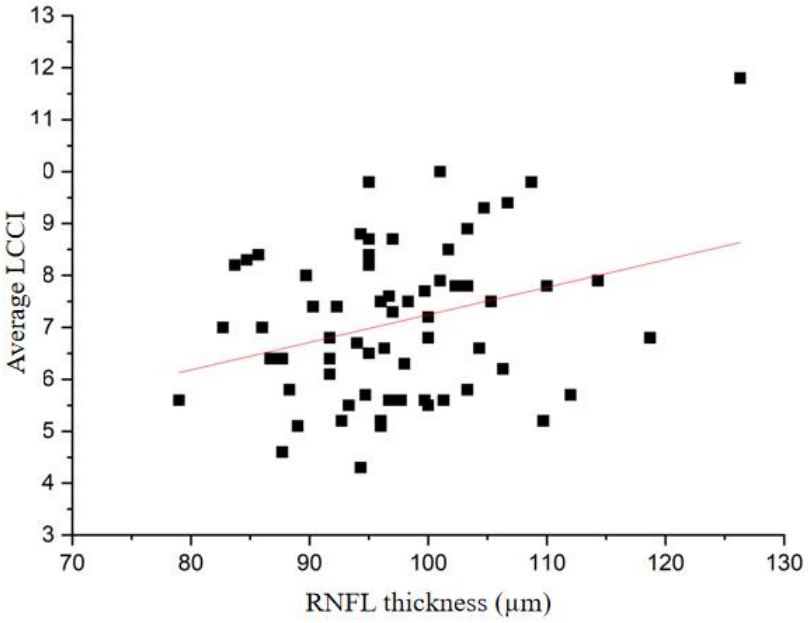

Figure 3.10. Scatter plot showing that the RNFL thickness had a positive association with the Average LCCI. Pearson correlation coefficient (r) = 0.307, p = 0.014.

3.3 Discussion

The interobserver reproducibility was excellent with similar limits of agreement as with those reported by previous studies (Kim et al., 2020; Lee et al., 2019). As mentioned above, the biomechanical properties of the LC can be represented by its morphology such as LCCI (Kim et al., 2019; Lee et al., 2016). Eyes with larger LCCI may be more prone to glaucomatous damage (Kim et al., 2018). Study 1 demonstrated that the IOP was unstable during the ocular compression. This means that investigators would not know the exact amount of IOP elevation when LC anterior surface was deformed during the ocular compression. Therefore, LCCI as a static parameter to represent the biomechanics of LC was applied in Study 2. Measurements of both corneal and LC biomechanics are challenging in clinical practice. Only one study has reported simultaneous measurement of CH and LCCI (Lee et al., 2019). These researchers recruited 65 POAG patients and randomly selected one eye in each patient for CH and LCCI measurements. They have found that eyes with higher LCCI had lower CH and higher IOPcc. However, LCCI showed no significant correlation with RNFL thickness or AL. Therefore, researchers proposed that the association of LCCI and CH could be explained by sharing similar collagen. It also could be hypothesized that the biomechanical properties of both LC and the cornea are acquired after birth. Any unusual pressure within the eyeball could affect both ends of the scleral canal (cornea and LC). However, no healthy subjects were included in their study, thus, the correlation between CH and LCCI could not be studied.

Consistent with the study by Hon et al. (2017), HM had lower CH and lower normalized tangent modulus as compared with LM. Regarding LCCI, a higher LCCI may indicate a higher glaucoma risk. Kim et al. (2020) found that eyes with greater LCCI had a faster rate of RNFL loss in patients with suspected glaucoma. Kim et al. (2019) reported that patients with unilateral NTG had higher LCCI (9.28 ± 1.62) in the affected than the fellow normal eye (7.67 ± 1.31). Eyes with NTG had higher LCCI (9.79 ± 1.36) than OHT (7.24 ± 1.29) than normal subjects (7.04 ± 1.31) (Kim

et al., 2020). IOP in the normal range did not influence LCCI. Although having a safe IOP level, a healthy eye with a higher LCCI may have a higher risk to develop glaucoma. There has been one study evaluating LCCI in healthy subjects. Lee et al. (2019) found that average LCCI in subjects aged 20 to 83 years old was 7.46 ± 1.22. This is similar to the average LCCI of all eyes (7.11 ± 1.50) in the current study (Table 3.2). There was a significant difference found in the Average LCCI between HM (6.37 ± 1.05) and LM (7.84 ± 1.54). Although older subjects and shorter eyes had a larger LCCI, only the axial length was significantly associated with LCCI in a multivariate analysis (Lee et al., 2019). Around 22% of the subjects included in the study conducted by Lee et al. (2019) had other systemic problems, including diabetes mellitus or systemic hypertension. From both the previous and current studies, LCCI might not be a good indicator of glaucoma risk at least in eyes with high myopia. Although HM had a lower average LCCI, their LCCI could still be increased if glaucoma further develops. Horizontal LC curvature would become steeper in the NTG and would further steepen in high-pressure glaucoma (Kim et al., 2016). Therefore, the LCCI of HM should be continuously monitored regardless of an initial low average LCCI. Longitudinal monitoring of LCCI is recommended rather than a snapshot LCCI measurement in HM.

HM had a more flattened anterior LC surface than LM. There was a significant difference in LCCI in the superior and mid-horizontal ONH in the LM, whereas the LCCI values of the three regions were similar and lower in HM. The mid-LCD of HM was significantly smaller than LM in all three regions (Table 3.2). In addition, the two groups had similar Max-LCD. This observation is consistent with previous studies (Kim et al., 2018; Lee et al., 2018, 2018), suggesting that axial elongation stretched and flattened LC curvature without changing BMO location, size, and depth (Figure 3.11).

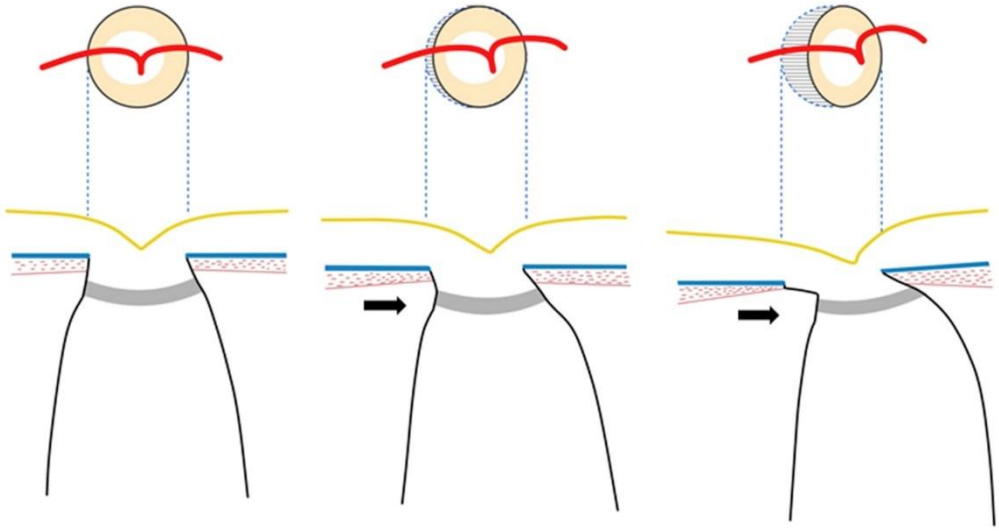

Figure 3.11. Schematic illustration showing the changes in the LC during axial elongation (Kim et al., 2018). LC (gray plate) was stretched in a nasal direction and became flattened**.**

Consistent with previous studies (Kim et al., 2019; Kim et al., 2019; Seo et al., 2014), LCD was the largest in the superior plane in this study. According to Kim et al. (2018), the glaucomatous eyes had the largest LCD in the superior region. This may be due to the superior plane having greater choroid thickness than the inferior regions (Ikuno et al., 2010). The clinical results of all subjects in the three different regions showed that LCCI in the mid-horizontal plane was the smallest. Previous studies (Lee et al., 2019; Seo et al., 2014) revealed that there was a horizontal central ridge in the LC center leading to a lower LCCI. Since the superior and inferior regions of the LC contained larger pores and thinner connective tissues than the other regions (Jonas et al., 1991), these two planes were more deformable and more susceptible to glaucomatous damage. In addition, the LC would be stretched more along the inferior-superior direction than in other directions under high IOP, which could result in the

development of axonal damages in these two regions (Midgett et al., 2017). Mid-horizontal planes had the smallest LCCI as compared with other planes, while there was no statistically significant difference between middle and inferior planes. This is likely because all subjects are healthy with young myopes with normal IOP and RNFL thickness, and no history of glaucoma. Some studies (Kim et al., 2020; Kim et al., 2020) measured the LCCI at seven equidistance planes from the two ends of the vertical ONH. However, the effect of glaucomatous damage would be averaged and alleviated if more planes are evaluated (Lee et al., 2018).

Regarding the association of average LCCI with other ocular parameters, LCCI was negatively associated with AL and IOPcc (Table 3.3). It was also marginally associated with CH and RNFL thickness. However, in multivariate analysis, only AL was still significantly associated with LCCI. Although Lee et al. (2019) found a negative association between CH and LCCI in POAG ($r = -0.411$, $p < 0.001$), their subjects suffered from glaucoma in contrast to the healthy subjects in the current study. Corneal tangent modulus had no significant association with LCCI. Possibly because the CH and tangent modulus are evaluations of tissue properties of the cornea, whereas the LCCI is an evaluation of the LC morphology. It would be ideal if the LC biomechanical properties could be measured directly.

In terms of both CH and tangent modulus in healthy subjects with different refractive errors, this is the first study on the associations between LCCI and corneal biomechanical properties. Although previous studies have advocated the usefulness of LCCI to predict LC deformations from glaucomatous damage, LCCI may have limited usage in eyes with high myopia.

This study has some limitations. First, the current study only involved young myopic Chinese. The findings may not be generalizable to other ethnic groups. Second, the

measurements of LCCI were obtained manually. It would be ideal if an algorithm could be developed to delineate the anterior LC surface to derive the LCCI objectively.

4. Conclusions and future direction

Previous studies have used ocular compression to elevate IOP and monitor LC shape using SD-OCT. Study 1 has confirmed that the IOP was not constant during the ocular compression. Thus, a single IOP measurement at the beginning of OCT acquisition is inappropriate. Researchers may take an average result from two IOP readings obtained at the beginning and at the end of the OCT acquisition to represent IOP elevation. Since high myopes and low myopes had different IOP profile changes during and after the ocular compression, further studies are warranted to determine if this difference could be related to aqueous outflow facilities.

In addition, although LCCI was found to be higher in glaucomatous eyes than with normal subjects, healthy high myopes have a smaller LCCI, which is likely caused by the stretching of the ONH tissues during axial elongation. When high myopes develop into glaucoma, their LCCI could be increased to a similar level to that of healthy low myopes. A longitudinal study would be required to confirm this hypothesis. LCCI may not be a good parameter to indicate the risk of glaucoma in high myopes. A better index is required to indicate the biomechanical properties of the LC rather than just measuring its shape.

References

Abitbol, O., Bouden, J., Doan, S., Hoang-Xuan, T., & Gatinel, D. (2010). Corneal hysteresis measured with the ocular response analyzer® in normal and glaucomatous eyes. Acta ophthalmologica, 88(1), 116-119.

Abu-Hassan, D. W., Li, X., Ryan, E. I., Acott, T. S., & Kelley, M. J. (2015). Induced pluripotent stem cells restore function in a human cell loss model of open-angle glaucoma. Stem cells, 33(3), 751-761.

Acott, T. S., Kelley, M. J., Keller, K. E., Vranka, J. A., Abu-Hassan, D. W., Li, X., Aga, M., & Bradley, J. M. (2014). Intraocular pressure homeostasis: maintaining balance in a high-pressure environment. Journal of Ocular pharmacology and therapeutics, 30(2-3), 94-101.

Agoumi, Y., Sharpe, G. P., Hutchison, D. M., Nicolela, M. T., Artes, P. H., & Chauhan, B. C. (2011). Laminar and prelaminar tissue displacement during intraocular pressure elevation in glaucoma patients and healthy controls. Ophthalmology, 118(1), 52-59.

Agoumi, Y., Sharpe, G. P., Hutchison, D. M., Nicolela, M. T., Artes, P. H., & Chauhan, B. C. (2011). Laminar and Prelaminar Tissue Displacement During Intraocular Pressure Elevation in Glaucoma Patients and Healthy Controls. Ophthalmology, 118(1), 52-59.

Al-Mezaine, H. S., Al-Obeidan, S., Kangave, D., Sadaawy, A., Wehaib, T. A., & Al-Amro, S. A. (2009). The relationship between central corneal thickness and degree of myopia among Saudi adults. International ophthalmology, 29(5), 373-378.

Albon, J., Karwatowski, W., Avery, N., Easty, D. L., & Duance, V. C. (1995). Changes in the collagenous matrix of the aging human lamina cribrosa. British journal of ophthalmology, 79(4), 368-375.

Ang, G. S., Bochmann, F., Townend, J., & Azuara-Blanco, A. (2008). Corneal biomechanical properties in primary open angle glaucoma and normal tension glaucoma. Journal of glaucoma, 17(4), 259-262.

Arumugam, B., Hung, L.-F., To, C.-h., Holden, B., & Smith, E. L. (2014). The effects of simultaneous dual focus lenses on refractive development in infant monkeys. Investigative Ophthalmology & Visual Science, 55(11), 7423-7432.

Ashby, R. S., & Schaeffel, F. (2010). The effect of bright light on lens compensation in chicks. Investigative Ophthalmology & Visual Science, 51(10), 5247-5253.

Asrani, S., Zeimer, R., Wilensky, J., Gieser, D., Vitale, S., & Lindenmuth, K. (2000). Large diurnal fluctuations in intraocular pressure are an independent risk factor in patients with glaucoma. Journal of glaucoma, 9(2), 134-142.

Bedggood, P., Tanabe, F., McKendrick, A. M., Turpin, A., Anderson, A. J., & Bui, B. V. (2018). Optic nerve tissue displacement during mild intraocular pressure elevation: its relationship to central corneal thickness and corneal hysteresis. Ophthalmic and Physiological Optics, 38(4), 389-399.

Bellezza, A. J., Rintalan, C. J., Thompson, H. W., Downs, J. C., Hart, R. T., & Burgoyne, C. F. (2003). Deformation of the lamina cribrosa and anterior scleral canal wall in early

experimental glaucoma. Investigative Ophthalmology & Visual Science, 44(2), 623-637.

Bengtsson, B., Leske, M. C., Hyman, L., Heijl, A., & Group, E. M. G. T. (2007). Fluctuation of intraocular pressure and glaucoma progression in the early manifest glaucoma trial. Ophthalmology, 114(2), 205-209.

Beotra, M. R., Wang, X., Tun, T. A., Zhang, L., Baskaran, M., Aung, T., Strouthidis, N. G., & Girard, M. J. (2018). In vivo three-dimensional lamina cribrosa strains in healthy, ocular hypertensive, and glaucoma eyes following acute intraocular pressure elevation. Investigative Ophthalmology & Visual Science, 59(1), 260-272.

Bland, J. M., & Altman, D. G. (1996). Statistics notes: Measurement error proportional to the mean .23. British Medical Journal, 313(7049), 106-106. https://doi.org/DOI 10.1136/bmj.313.7049.106

Bonomi, L., Marchini, G., Marraffa, M., Bernardi, P., Morbio, R., & Varotto, A. (2000). Vascular risk factors for primary open angle glaucoma: the Egna-Neumarkt Study. Ophthalmology, 107(7), 1287-1293.

Boscia, F., Grattagliano, I., Vendemiale, G., Micelli-Ferrari, T., & Altomare, E. (2000). Protein oxidation and lens opacity in humans. Investigative Ophthalmology & Visual Science, 41(9), 2461-2465.

Bourne, R. R., Jonas, J. B., Bron, A. M., Cicinelli, M. V., Das, A., Flaxman, S. R., Friedman, D. S., Keeffe, J. E., Kempen, J. H., & Leasher, J. (2018). Prevalence and causes of vision loss in high-income countries and in Eastern and Central Europe in 2015: magnitude, temporal trends and projections. British journal of ophthalmology, 102(5), 575-585.

Bueno-Gimeno, I., España-Gregori, E., Gene-Sampedro, A., Lanzagorta-Aresti, A., & Piñero-Llorens, D. P. (2014). Relationship among corneal biomechanics, refractive error, and axial length. Optometry and vision science, 91(5), 507-513.

Buzard, K. A. (1992). Introduction to biomechanics of the cornea. Refract Corneal Surg, 8(2), 127-138.

Cantor, E., Méndez, F., Rivera, C., Castillo, A., & Martínez-Blanco, A. (2018). Blood pressure, ocular perfusion pressure and open-angle glaucoma in patients with systemic hypertension. Clinical ophthalmology (Auckland, NZ), 12, 1511.

Cao, K., Wan, Y., Yusufu, M., & Wang, N. (2020). Significance of outdoor time for myopia prevention: a systematic review and meta-analysis based on randomized controlled trials. Ophthalmic research, 63(2), 97-105.

Caprioli, J., & Coleman, A. L. (2008). Intraocular pressure fluctuation: a risk factor for visual field progression at low intraocular pressures in the Advanced Glaucoma Intervention Study. Ophthalmology, 115(7), 1123-1129. e1123.

Chang, S.-W., Tsai, I.-L., Hu, F.-R., Lin, L. L.-K., & Shih, Y.-F. (2001). The cornea in young myopic adults. British journal of ophthalmology, 85(8), 916-920.

Chen, H., Lin, H., Lin, Z., Chen, J., & Chen, W. (2016). Distribution of axial length, anterior chamber depth, and corneal curvature in an aged population in South China. BMC ophthalmology, 16(1), 1-7.

Chen, M., Wu, A., Zhang, L., Wang, W., Chen, X., Yu, X., & Wang, K. (2018). The increasing prevalence of myopia and high myopia among high school students in Fenghua city, eastern China: a 15-year population-based survey. BMC ophthalmology, 18(1), 1-10.

Chen, S.-J., Lu, P., Zhang, W.-F., & Lu, J.-H. (2012). High myopia as a risk factor in primary open angle glaucoma. International journal of ophthalmology, 5(6), 750.

Chen, W., Hu, T., Xu, Q., Chen, Z., Zhang, H., & Wang, J. (2020). Acute effects of intraocular pressure-induced changes in schlemm's canal morphology on outflow facility in healthy human eyes. Investigative Ophthalmology & Visual Science, 61(8), 36-36.

Chen, W., Hu, T., Xu, Q. F., Chen, Z. Q., Zhang, H., & Wang, J. M. (2020). Acute Effects of Intraocular Pressure-Induced Changes in Schlemm's Canal Morphology on Outflow Facility in Healthy Human Eyes. Investigative Ophthalmology & Visual Science, 61(8).

Chen, Z., Song, Y., Li, M., Chen, W., Liu, S., Cai, Z., Chen, L., Xiang, Y., Zhang, H., & Wang, J. (2018). Schlemm's canal and trabecular meshwork morphology in high myopia. Ophthalmic and Physiological Optics, 38(3), 266-272.

Cho, B.-J., Shin, J. Y., & Yu, H. G. (2016). Complications of pathologic myopia. Eye & contact lens, 42(1), 9-15.

Choi, K. Y., Mok, A. Y. t., Do, C. w., Lee, P. H., & Chan, H. H. l. (2020). The diversified defocus profile of the near-work environment and myopia development. Ophthalmic and Physiological Optics, 40(4), 463-471.

Chua, S. Y., Sabanayagam, C., Cheung, Y. B., Chia, A., Valenzuela, R. K., Tan, D., Wong, T. Y., Cheng, C. Y., & Saw, S. M. (2016). Age of onset of myopia predicts risk of high myopia in later childhood in myopic Singapore children. Ophthalmic and Physiological Optics, 36(4), 388-394.

De Moraes, C. V. G., Hill, V., Tello, C., Liebmann, J. M., & Ritch, R. (2012). Lower corneal hysteresis is associated with more rapid glaucomatous visual field progression. Journal of glaucoma, 21(4), 209-213.

Dennis, Y. T., Lam, C. S., Guggenheim, J. A., Lam, C., Li, K.-k., Liu, Q., & To, C.-h. (2007). Simultaneous defocus integration during refractive development. Investigative Ophthalmology & Visual Science, 48(12), 5352-5359.

Dirani, M., Tong, L., Gazzard, G., Zhang, X., Chia, A., Young, T. L., Rose, K. A., Mitchell, P., & Saw, S.-M. (2009). Outdoor activity and myopia in Singapore teenage children. British journal of ophthalmology, 93(8), 997-1000.

Dong, J., Zhang, Y., Zhang, H., Jia, Z., Zhang, S., Sun, B., Han, Y., & Wang, X. (2018). Corneal densitometry in high myopia. BMC ophthalmology, 18(1), 1-6.

Downs, J. C., Roberts, M. D., & Burgoyne, C. F. (2008). The mechanical environment of the optic nerve head in glaucoma. Optometry and vision science: official publication of the American Academy of Optometry, 85(6), 425.

Elsheikh, A., McMonnies, C. W., Whitford, C., & Boneham, G. C. (2015). In vivo study of corneal responses to increased intraocular pressure loading. Eye and vision, 2(1), 1-10.

Fam, H.-B., How, A. C., Baskaran, M., Lim, K.-L., Chan, Y.-H., & Aung, T. (2006). Central corneal thickness and its relationship to myopia in Chinese adults. British journal of ophthalmology, 90(12), 1451-1453.

Fechtner, R. D., & Weinreb, R. N. (1994). Mechanisms of optic nerve damage in primary open angle glaucoma. Survey of ophthalmology, 39(1), 23-42.

Feldkaemper, M., & Schaeffel, F. (2013). An updated view on the role of dopamine in myopia. Experimental eye research, 114, 106-119.

Fernández-Barrientos, Y., García-Feijoó, J., Martínez-de-la-Casa, J. M., Pablo, L. E., Fernández-Pérez, C., & Sánchez, J. G. (2010). Fluorophotometric study of the effect of the glaukos trabecular microbypass stent on aqueous humor dynamics. Investigative Ophthalmology & Visual Science, 51(7), 3327-3332.

Flammer, J. (1994). The vascular concept of glaucoma. Survey of ophthalmology, 38, S3-S6.

Flammer, J., Orgül, S., Costa, V. P., Orzalesi, N., Krieglstein, G. K., Serra, L. M., Renard, J.-P., & Stefánsson, E. (2002). The impact of ocular blood flow in glaucoma. Progress in retinal and eye research, 21(4), 359-393.

Flitcroft, D. I., He, M., Jonas, J. B., Jong, M., Naidoo, K., Ohno-Matsui, K., Rahi, J., Resnikoff, S., Vitale, S., & Yannuzzi, L. (2019). IMI–Defining and classifying myopia: a proposed set of standards for clinical and epidemiologic studies. Investigative ophthalmology & visual science, 60(3), M20-M30.

Foulds, W. S., Barathi, V. A., & Luu, C. D. (2013). Progressive myopia or hyperopia can be induced in chicks and reversed by manipulation of the chromaticity of ambient light. Investigative Ophthalmology & Visual Science, 54(13), 8004-8012.

Garcia-Porta, N., Fernandes, P., Queiros, A., Salgado-Borges, J., Parafita-Mato, M., & González-Méijome, J. M. (2014). Corneal biomechanical properties in different ocular conditions and new measurement techniques. International Scholarly Research Notices, 2014.

Gatzioufas, Z., Labiris, G., Stachs, O., Hovakimyan, M., Schnaidt, A., Viestenz, A., Käsmann-Kellner, B., & Seitz, B. (2013). Biomechanical profile of the cornea in primary congenital glaucoma. Acta ophthalmologica, 91(1), e29-e34.

Girard, M. J., Strouthidis, N. G., Ethier, C. R., & Mari, J. M. (2011). Shadow removal and contrast enhancement in optical coherence tomography images of the human optic nerve head. Investigative Ophthalmology & Visual Science, 52(10), 7738-7748.

Grise-Dulac, A., Saad, A., Abitbol, O., Febbraro, J.-L., Azan, E., Moulin-Tyrode, C., & Gatinel, D. (2012). Assessment of corneal biomechanical properties in normal tension glaucoma and comparison with open-angle glaucoma, ocular hypertension, and normal eyes. Journal of glaucoma, 21(7), 486-489.

Guo, T., Sampathkumar, S., Fan, S., Morris, N., Wang, F., & Toris, C. B. (2017). Aqueous humour dynamics and biometrics in the ageing Chinese eye. British journal of ophthalmology, 101(9), 1290-1296.

Guo, Y., Liu, L. J., Xu, L., Lv, Y. Y., Tang, P., Feng, Y., Meng, M., & Jonas, J. B. (2013). Outdoor activity and myopia among primary students in rural and urban regions of Beijing. Ophthalmology, 120(2), 277-283.

Gupta, N., & Weinreb, R. N. (1997). New definitions of glaucoma. Current opinion in ophthalmology, 8(2), 38-41.

Haarman, A. E., Enthoven, C. A., Tideman, J. W. L., Tedja, M. S., Verhoeven, V. J., & Klaver, C. C. (2020). The complications of myopia: a review and meta-analysis. Investigative Ophthalmology & Visual Science, 61(4), 49-49.

Hayashi, K., Ohno-Matsui, K., Shimada, N., Moriyama, M., Kojima, A., Hayashi, W., Yasuzumi, K., Nagaoka, N., Saka, N., & Yoshida, T. (2010). Long-term pattern of progression of myopic maculopathy: a natural history study. Ophthalmology, 117(8), 1595-1611. e1594.

He, M., Wang, W., Ding, H., & Zhong, X. (2017). Corneal biomechanical properties in high

myopia measured by dynamic scheimpflug imaging technology. Optometry and vision science, 94(12), 1074-1080.

Heijl, A., Leske, M. C., Bengtsson, B., Hyman, L., Bengtsson, B., Hussein, M., & Group, E. M. G. T. (2002). Reduction of intraocular pressure and glaucoma progression: results from the Early Manifest Glaucoma Trial. Archives of ophthalmology, 120(10), 1268-1279.

Holden, B. A., Fricke, T. R., Wilson, D. A., Jong, M., Naidoo, K. S., Sankaridurg, P., Wong, T. Y., Naduvilath, T. J., & Resnikoff, S. (2016). Global prevalence of myopia and high myopia and temporal trends from 2000 through 2050. Ophthalmology, 123(5), 1036-1042.

Holekamp, N. M. (2010). The vitreous gel: more than meets the eye. American Journal of Ophthalmology, 149(1), 32-36. e31.

Holekamp, N. M., Harocopos, G. J., Shui, Y.-B., & Beebe, D. C. (2008). Myopia and axial length contribute to vitreous liquefaction and nuclear cataract. Archives of ophthalmology, 126(5), 744.

Hon, Y., Chen, G.-Z., Lu, S.-H., Lam, D. C., & Lam, A. K. (2017). In vivo measurement of regional corneal tangent modulus. Scientific reports, 7(1), 1-8.

Hon, Y., Chen, G.-Z., Lu, S.-H., Lam, D. C. C., & Lam, A. K. C. (2017). High myopes have lower normalised corneal tangent moduli (less 'stiff' corneas) than low myopes. Ophthalmic and Physiological Optics, 37(1), 42-50.

Hon, Y., Wan, K., Chen, G.-Z., Lu, S.-H., Lam, D. C., & Lam, A. K. (2016). Diurnal variation of corneal tangent modulus in normal Chinese. Cornea, 35(12), 1600-1604.

Hou, W., Norton, T. T., Hyman, L., Gwiazda, J., & Group, C. (2018). Axial elongation in myopic children and its association with myopia progression in the Correction of Myopia Evaluation Trial (COMET). Eye & contact lens, 44(4), 248.

Huang, H.-M., Chang, D. S.-T., & Wu, P.-C. (2015). The association between near work activities and myopia in children—a systematic review and meta-analysis. PLoS One, 10(10), e0140419.

Huang, W., Fan, Q., Wang, W., Zhou, M., Laties, A. M., & Zhang, X. (2013). Collagen: a potential factor involved in the pathogenesis of glaucoma. Medical science monitor basic research, 19, 237.

Hyman, L., Gwiazda, J., Hussein, M., Norton, T. T., Wang, Y., Marsh-Tootle, W., & Everett, D. (2005). Relationship of age, sex, and ethnicity with myopia progression and axial elongation in the correction of myopia evaluation trial. Arch Ophthalmol, 123(7), 977-987.

Ikuno, Y., Kawaguchi, K., Nouchi, T., & Yasuno, Y. (2010). Choroidal thickness in healthy Japanese subjects. Investigative Ophthalmology & Visual Science, 51(4), 2173-2176.

Inamori, Y., Ota, M., Inoko, H., Okada, E., Nishizaki, R., Shiota, T., Mok, J., Oka, A., Ohno, S., & Mizuki, N. (2007). The COL1A1 gene and high myopia susceptibility in Japanese. Human genetics, 122(2), 151-157.

Ip, J. M., Huynh, S. C., Robaei, D., Rose, K. A., Morgan, I. G., Smith, W., Kifley, A., & Mitchell, P. (2007). Ethnic differences in the impact of parental myopia: findings from a population-based study of 12-year-old Australian children. Investigative Ophthalmology & Visual Science, 48(6), 2520-2528.

Ip, J. M., Saw, S.-M., Rose, K. A., Morgan, I. G., Kifley, A., Wang, J. J., & Mitchell, P. (2008).

Role of near work in myopia: findings in a sample of Australian school children. Investigative Ophthalmology & Visual Science, 49(7), 2903-2910.

Iwase, T., Akahori, T., Yamamoto, K., Ra, E., & Terasaki, H. (2018). Evaluation of optic nerve head blood flow in response to increase of intraocular pressure. Scientific reports, 8(1), 1-11.

Jammal, A. A., Berchuck, S. I., Mariottoni, E. B., Tanna, A. P., Costa, V. P., & Medeiros, F. A. (2022). Blood Pressure and Glaucomatous Progression in a Large Clinical Population. Ophthalmology, 129(2), 161-170.

Johnstone, J., Fazio, M., Rojananuangnit, K., Smith, B., Clark, M., Downs, C., Owsley, C., Girard, M. J., Mari, J. M., & Girkin, C. A. (2014). Variation of the axial location of Bruch's membrane opening with age, choroidal thickness, and race. Investigative Ophthalmology & Visual Science, 55(3), 2004-2009.

Johnstone, M. A. (2014). Intraocular pressure regulation: findings of pulse-dependent trabecular meshwork motion lead to unifying concepts of intraocular pressure homeostasis. In (Vol. 30, pp. 88-93): Mary Ann Liebert, Inc. 140 Huguenot Street, 3rd Floor New Rochelle, NY 10801 USA.

Jonas, J., Budde, W., Stroux, A., Oberacher-Velten, I., & Jünemann, A. (2007). Diurnal intraocular pressure profiles and progression of chronic open-angle glaucoma. Eye, 21(7), 948-951.

Jonas, J., Mardin, C. Y., Schlötzer-Schrehardt, U., & Naumann, G. (1991). Morphometry of the human lamina cribrosa surface. Investigative Ophthalmology & Visual Science, 32(2), 401-405.

Jones, D., & Luensmann, D. (2012). The prevalence and impact of high myopia. Eye & contact lens, 38(3), 188-196.

Kadziauskienė, A., Jašinskienė, E., Ašoklis, R., Lesinskas, E., Rekašius, T., Chua, J., Cheng, C.-Y., Mari, J. M., Girard, M. J., & Schmetterer, L. (2018). Long-term shape, curvature, and depth changes of the lamina cribrosa after trabeculectomy. Ophthalmology, 125(11), 1729-1740.

Kang, B. S., Wang, L.-K., Zheng, Y.-P., Guggenheim, J. A., Stell, W. K., & Kee, C.-s. (2018). High myopia induced by form deprivation is associated with altered corneal biomechanical properties in chicks. Plos One, 13(11), e0207189.

Kanthan, G. L., Mitchell, P., Rochtchina, E., Cumming, R. G., & Wang, J. J. (2014). Myopia and the long-term incidence of cataract and cataract surgery: the B lue M ountains E ye S tudy. Clinical & experimental ophthalmology, 42(4), 347-353.

Karyotakis, N. G., Ginis, H. S., Dastiridou, A. I., Tsilimbaris, M. K., & Pallikaris, I. G. (2015). Manometric measurement of the outflow facility in the living human eye and its dependence on intraocular pressure. Acta ophthalmologica, 93(5), e343-e348.

Kaushik, S., Pandav, S. S., Banger, A., Aggarwal, K., & Gupta, A. (2012). Relationship between corneal biomechanical properties, central corneal thickness, and intraocular pressure across the spectrum of glaucoma. American Journal of Ophthalmology, 153(5), 840-849. e842.

Kim, G.-N., Kim, J.-A., Kim, M.-J., Lee, E. J., Hwang, J.-M., & Kim, T.-W. (2020). Comparison of lamina cribrosa morphology in normal tension glaucoma and autosomal-dominant

optic atrophy. Investigative Ophthalmology & Visual Science, 61(5), 9-9.

Kim, J.-A., Kim, T.-W., Lee, E. J., Girard, M. J., & Mari, J. M. (2019). Lamina cribrosa morphology in glaucomatous eyes with hemifield defect in a Korean population. Ophthalmology, 126(5), 692-701.

Kim, J.-A., Kim, T.-W., Lee, E. J., Girard, M. J., & Mari, J. M. (2020). Comparison of lamina cribrosa morphology in eyes with ocular hypertension and normal-tension glaucoma. Investigative Ophthalmology & Visual Science, 61(4), 4-4.

Kim, J.-A., Kim, T.-W., Lee, E. J., Girard, M. J., & Mari, J. M. (2020). Relationship between lamina cribrosa curvature and the microvasculature in treatment-naïve eyes. British journal of ophthalmology, 104(3), 398-403.

Kim, J.-A., Kim, T.-W., Lee, E. J., Kim, J. M., Girard, M. J., & Mari, J. M. (2019). Intereye comparison of lamina cribrosa curvature in normal tension glaucoma patients with unilateral damage. Investigative Ophthalmology & Visual Science, 60(7), 2423-2430.

Kim, J.-A., Kim, T.-W., Weinreb, R. N., Lee, E. J., Girard, M. J., & Mari, J. M. (2018). Lamina cribrosa morphology predicts progressive retinal nerve fiber layer loss in eyes with suspected glaucoma. Scientific reports, 8(1), 1-10.

Kim, J.-A., Lee, E. J., Kim, T.-W., Kim, H., Girard, M. J. A., Mari, J. M., Yang, H. K., & Hwang, J.-M. (2020). Differentiation of nonarteritic anterior ischemic optic neuropathy from normal tension glaucoma by comparison of the lamina cribrosa. Investigative Ophthalmology & Visual Science, 61(8), 21-21.

Kim, J. A., Kim, T. W., Lee, E. J., Kim, J. M., Girard, M. J. A., & Mari, J. M. (2019). Intereye Comparison of Lamina Cribrosa Curvature in Normal Tension Glaucoma Patients With Unilateral Damage. Investigative Ophthalmology & Visual Science, 60(7), 2423-2430.

Kim, M., Choung, H.-K., Lee, K. M., Oh, S., & Kim, S. H. (2018). Longitudinal changes of optic nerve head and peripapillary structure during childhood myopia progression on OCT: Boramae Myopia Cohort Study Report 1. Ophthalmology, 125(8), 1215-1223.

Kim, Y. W., Jeoung, J. W., Girard, M. J., Mari, J. M., & Park, K. H. (2016). Positional and curvature difference of lamina cribrosa according to the baseline intraocular pressure in primary open-angle glaucoma: a swept-source optical coherence tomography (SS-OCT) study. PLoS One, 11(9), e0162182.

King, A., Azuara-Blanco, A., & Tuulonen, A. (2013). Glaucoma. Bmj, 346, f3518. https://doi.org/10.1136/bmj.f3518

Ko, M. W., Leung, L. K., Lam, D. C., & Leung, C. K. (2013). Characterization of corneal tangent modulus in vivo. Acta Ophthalmol, 91(4), e263-269. https://doi.org/10.1111/aos.12066

Ko, M. W. L., Leung, L. K. K., Lam, D. C. C., & Leung, C. K. S. (2013). Characterization of corneal tangent modulus in vivo. Acta ophthalmologica, 91(4), E263-E269.

Lam, A. K., Hon, Y., Leung, L. K., & Lam, D. C. (2015). Repeatability of a novel corneal indentation device for corneal biomechanical measurement. Ophthalmic Physiol Opt, 35(4), 455-461.

Lam, A. K., Hon, Y., Leung, L. K., & Lam, D. C. (2015). Repeatability of a novel corneal indentation device for corneal biomechanical measurement. Ophthalmic and Physiological Optics, 35(4), 455-461.

Lam, A. K. C., Chen, D., & Tse, J. (2010). The Usefulness of Waveform Score from the Ocular

Response Analyzer. Optometry and vision science, 87(3), 195-199.

Lam, C. S. Y., Tang, W. C., Tse, D. Y.-y., Lee, R. P. K., Chun, R. K. M., Hasegawa, K., Qi, H., Hatanaka, T., & To, C. H. (2020). Defocus Incorporated Multiple Segments (DIMS) spectacle lenses slow myopia progression: a 2-year randomised clinical trial. British journal of ophthalmology, 104(3), 363-368.

Lam, C. S. Y., Tang, W. C., Tse, D. Y.-Y., Tang, Y. Y., & To, C. H. (2014). Defocus Incorporated Soft Contact (DISC) lens slows myopia progression in Hong Kong Chinese schoolchildren: a 2-year randomised clinical trial. British journal of ophthalmology, 98(1), 40-45.

Lam, D. S. C., Leung, D. Y. L., Chiu, T. Y. H., Fan, D. S. P., Cheung, E. Y. Y., Wong, T. Y., Lai, J. S. M., & Tham, C. C. Y. (2004). Pressure phosphene self-tonometry: A comparison with Goldmann tonometry in glaucoma patients. Investigative Ophthalmology & Visual Science, 45(9), 3131-3136.

Lam, K. C. A., Wong, H. Y., Hon, Y., & Wang, X. (2019). Acute transient intraocular pressure elevation through ProviewTM eye pressure monitor. Annual Meeting and 3rd World Congress of Optometry, American Academy of Optometry (AAO),

Lanzagorta-Aresti, A., Perez-Lopez, M., Palacios-Pozo, E., & Davo-Cabrera, J. (2017). Relationship between corneal hysteresis and lamina cribrosa displacement after medical reduction of intraocular pressure. British Journal of Ophthalmology, 101(3), 290-294.

Lee, E. J., Kim, T.-W., Kim, H., Lee, S. H., Girard, M. J., & Mari, J. M. (2018). Comparison between lamina cribrosa depth and curvature as a predictor of progressive retinal nerve fiber layer thinning in primary open-angle glaucoma. Ophthalmology Glaucoma, 1(1), 44-51.

Lee, E. J., Kim, T.-W., & Weinreb, R. N. (2013). Variation of lamina cribrosa depth following trabeculectomy. Investigative Ophthalmology & Visual Science, 54(8), 5392-5399.

Lee, E. J., Kim, T.-W., Weinreb, R. N., Park, K. H., Kim, S. H., & Kim, D. M. (2011). Visualization of the lamina cribrosa using enhanced depth imaging spectral-domain optical coherence tomography. American Journal of Ophthalmology, 152(1), 87-95. e81.

Lee, J. Y., Sung, K. R., Han, S., & Na, J. H. (2015). Effect of myopia on the progression of primary open-angle glaucoma. Investigative Ophthalmology & Visual Science, 56(3), 1775-1781.

Lee, K. M., Choung, H.-K., Kim, M., Oh, S., & Kim, S. H. (2018). Change of β-zone Parapapillary atrophy during axial elongation: Boramae myopia cohort study report 3. Investigative Ophthalmology & Visual Science, 59(10), 4020-4030.

Lee, K. M., Choung, H.-K., Kim, M., Oh, S., & Kim, S. H. (2018). Positional change of optic nerve head vasculature during axial elongation as evidence of lamina cribrosa shifting: Boramae Myopia Cohort Study Report 2. Ophthalmology, 125(8), 1224-1233.

Lee, K. M., Kim, T.-W., Lee, E. J., Girard, M. J., Mari, J. M., & Weinreb, R. N. (2019). Association of corneal hysteresis with lamina cribrosa curvature in primary open angle glaucoma. Investigative Ophthalmology & Visual Science, 60(13), 4171-4177.

Lee, P. P., Walt, J. W., Rosenblatt, L. C., Siegartel, L. R., Stern, L. S., & Group, G. C. S. (2007). Association between intraocular pressure variation and glaucoma progression: data from a United States chart review. American Journal of Ophthalmology, 144(6), 901-907.

e901.

Lee, S. H., Kim, T.-W., Lee, E. J., Girard, M. J., & Mari, J. M. (2017). Diagnostic power of lamina cribrosa depth and curvature in glaucoma. Investigative Ophthalmology & Visual Science, 58(2), 755-762.

Lee, S. H., Kim, T.-W., Lee, E. J., Girard, M. J., & Mari, J. M. (2019). Lamina cribrosa curvature in healthy Korean eyes. Scientific Reports, 9(1), 1-8.

Lee, S. H., Kim, T.-W., Lee, E. J., Girard, M. J., Mari, J. M., & Ritch, R. (2018). Ocular and clinical characteristics associated with the extent of posterior lamina cribrosa curve in normal tension glaucoma. Scientific Reports, 8(1), 1-9.

Lee, S. H., Yu, D. A., Kim, T. W., Lee, E. J., Girard, M. J., & Mari, J. M. (2016). Reduction of the Lamina Cribrosa Curvature After Trabeculectomy in Glaucoma. Invest Ophthalmol Vis Sci, 57(11), 5006-5014.

Lee, Y.-A., Shih, Y.-F., Lin, L. L.-K., Huang, J.-Y., & Wang, T.-H. (2008). Association between high myopia and progression of visual field loss in primary open-angle glaucoma. Journal of the Formosan Medical Association, 107(12), 952-957.

Leske, M. C., Heijl, A., Hussein, M., Bengtsson, B., Hyman, L., & Komaroff, E. (2003). Factors for glaucoma progression and the effect of treatment: the early manifest glaucoma trial. Archives of ophthalmology, 121(1), 48-56.

Leveziel, N., Marillet, S., Dufour, Q., Lichtwitz, O., Bentaleb, Y., Pelen, F., Ingrand, P., & Bourne, R. (2020). Prevalence of macular complications related to myopia–Results of a multicenter evaluation of myopic patients in eye clinics in France. Acta ophthalmologica, 98(2), e245-e251.

Li, S.-M., Wei, S., Atchison, D. A., Kang, M.-T., Liu, L., Li, H., Li, S., Yang, Z., Wang, Y., & Zhang, F. (2022). Annual Incidences and Progressions of Myopia and High Myopia in Chinese Schoolchildren Based on a 5-Year Cohort Study. Investigative Ophthalmology & Visual Science, 63(1), 8-8.

Li, Z., Liu, R., Xiao, O., Guo, X., Wang, D., Zhang, J., Ha, J. J., Lee, J. T. L., Lee, P., & Jong, M. (2019). Progression of myopic maculopathy in highly myopic Chinese eyes. Investigative Ophthalmology & Visual Science, 60(4), 1096-1104.

Lim, L., Gazzard, G., Chan, Y.-H., Fong, A., Kotecha, A., Sim, E.-L., Tan, D., Tong, L., & Saw, S.-M. (2008). Cornea biomechanical characteristics and their correlates with refractive error in Singaporean children. Investigative Ophthalmology & Visual Science, 49(9), 3852-3857.

Lin, L. L.-K., Shih, Y.-F., Hsiao, C. K., & Chen, C. (2004). Prevalence of myopia in Taiwanese schoolchildren: 1983 to 2000. Annals Academy of Medicine Singapore, 33(1), 27-33.

Lin, Z., Vasudevan, B., Jhanji, V., Mao, G. Y., Gao, T. Y., Wang, F. H., Rong, S. S., Ciuffreda, K. J., & Liang, Y. B. (2014). Near work, outdoor activity, and their association with refractive error. Optometry and vision science, 91(4), 376-382.

Long, E., Wu, X., Ding, X., Yang, Y., Wang, X., Guo, C., Zhang, X., Chen, K., Yu, T., & Wu, D. (2021). Real-world big data demonstrates prevalence trends and developmental patterns of myopia in China: A retrospective, multicenter study. Annals of Translational Medicine, 9(7).

Luce, D. A. (2005). Determining in vivo biomechanical properties of the cornea with an ocular

response analyzer. Journal of Cataract & Refractive Surgery, 31(1), 156-162.

Ma, J., Wang, Y., Wei, P., & Jhanji, V. (2018). Biomechanics and structure of the cornea: implications and association with corneal disorders. Survey of ophthalmology, 63(6), 851-861.

Mandalos, A., Anastasopoulos, E., Makris, L., Dervenis, N., Kilintzis, V., & Topouzis, F. (2013). Inter-examiner Reproducibility of Ocular Response Analyzer Using the Waveform Score Quality Index in Healthy Subjects. Journal of glaucoma, 22(2), 152-155.

Mari, J. M., Strouthidis, N. G., Park, S. C., & Girard, M. J. (2013). Enhancement of lamina cribrosa visibility in optical coherence tomography images using adaptive compensation. Investigative Ophthalmology & Visual Science, 54(3), 2238-2247.

Matlach, J., Bender, S., König, J., Binder, H., Pfeiffer, N., & Hoffmann, E. M. (2019). Investigation of intraocular pressure fluctuation as a risk factor of glaucoma progression. Clinical ophthalmology (Auckland, NZ), 13, 9.

Mayama, C., Suzuki, Y., Araie, M., Ishida, K., Akira, T., Yamamoto, T., Kitazawa, Y., Funaki, S., Shirakashi, M., & Abe, H. (2002). Myopia and advanced-stage open-angle glaucoma. Ophthalmology, 109(11), 2072-2077.

McBrien, N. A., Cornell, L. M., & Gentle, A. (2001). Structural and ultrastructural changes to the sclera in a mammalian model of high myopia. Investigative Ophthalmology & Visual Science, 42(10), 2179-2187.

McBrien, N. A., & Gentle, A. (2003). Role of the sclera in the development and pathological complications of myopia. Progress in retinal and eye research, 22(3), 307-338.

McBrien, N. A., Jobling, A. I., & Gentle, A. (2009). Biomechanics of the sclera in myopia: extracellular and cellular factors. Optometry and vision science, 86(1), E23-E30.

McCarthy, C., Megaw, P., Devadas, M., & Morgan, I. (2007). Dopaminergic agents affect the ability of brief periods of normal vision to prevent form-deprivation myopia. Experimental eye research, 84(1), 100-107.

McFadden, S. A., Dennis, Y. T., Bowrey, H. E., Leotta, A. J., Lam, C. S., Wildsoet, C. F., & To, C.-H. (2014). Integration of defocus by dual power Fresnel lenses inhibits myopia in the mammalian eye. Investigative Ophthalmology & Visual Science, 55(2), 908-917.

Medeiros, F. A., Meira-Freitas, D., Lisboa, R., Kuang, T.-M., Zangwill, L. M., & Weinreb, R. N. (2013). Corneal hysteresis as a risk factor for glaucoma progression: a prospective longitudinal study. Ophthalmology, 120(8), 1533-1540.

Meek, K., & Fullwood, N. J. (2001). Corneal and scleral collagens—a microscopist's perspective. Micron, 32(3), 261-272.

Meek, K. M., & Boote, C. (2004). The organization of collagen in the corneal stroma. Experimental eye research, 78(3), 503-512.

Micelli-Ferrari, T., Vendemiale, G., Grattagliano, I., Boscia, F., Arnese, L., Altomare, E., & Cardia, L. (1996). Role of lipid peroxidation in the pathogenesis of myopic and senile cataract. British journal of ophthalmology, 80(9), 840-843.

Midgett, D., Liu, B., Ling, Y. T. T., Jefferys, J. L., Quigley, H. A., & Nguyen, T. D. (2020). The effects of glaucoma on the pressure-induced strain response of the human lamina cribrosa. Investigative Ophthalmology & Visual Science, 61(4), 41-41.

Midgett, D. E., Pease, M. E., Jefferys, J. L., Patel, M., Franck, C., Quigley, H. A., & Nguyen, T. D.

(2017). The pressure-induced deformation response of the human lamina cribrosa: analysis of regional variations. Acta biomaterialia, 53, 123-139.

Mitchell, P., Hourihan, F., Sandbach, J., & Wang, J. J. (1999). The relationship between glaucoma and myopia: the Blue Mountains Eye Study. Ophthalmology, 106(10), 2010-2015.

Morgan, I. G., Ohno-Matsui, K., & Saw, S.-M. (2012). Myopia. The Lancet, 379(9827), 1739-1748.

Morgan, W. H., Balaratnasingam, C., Lind, C. R., Colley, S., Kang, M. H., House, P. H., & Yu, D.-Y. (2016). Cerebrospinal fluid pressure and the eye. British journal of ophthalmology, 100(1), 71-77.

Morita, T., Shoji, N., Kamiya, K., Fujimura, F., & Shimizu, K. (2012). Corneal biomechanical properties in normal-tension glaucoma. Acta ophthalmologica, 90(1), e48-e53.

Müller, L. J., Pels, E., Schurmans, L. R., & Vrensen, G. F. (2004). A new three-dimensional model of the organization of proteoglycans and collagen fibrils in the human corneal stroma. Experimental Eye Research, 78(3), 493-501.

Ohno-Matsui, K. (2016). Pathologic myopia. The Asia-Pacific Journal of Ophthalmology, 5(6), 415-423.

Pan, C.-W., Cheng, C.-y., Saw, S.-M., Wang, J. J., & Wong, T. Y. (2013). Myopia and age-related cataract: a systematic review and meta-analysis. American Journal of Ophthalmology, 156(5), 1021-1033. e1021.

Park, H.-Y. L., Jeon, S. H., & Park, C. K. (2012). Enhanced depth imaging detects lamina cribrosa thickness differences in normal tension glaucoma and primary open-angle glaucoma. Ophthalmology, 119(1), 10-20.

Park, H.-Y. L., & Park, C. K. (2013). Diagnostic capability of lamina cribrosa thickness by enhanced depth imaging and factors affecting thickness in patients with glaucoma. Ophthalmology, 120(4), 745-752.

Pillunat, K. R., Hermann, C., Spoerl, E., & Pillunat, L. E. (2016). Analyzing biomechanical parameters of the cornea with glaucoma severity in open-angle glaucoma. Graefe's Archive for Clinical and Experimental Ophthalmology, 254(7), 1345-1351.

Piñero, D. P., & Alcón, N. (2014). In vivo characterization of corneal biomechanics. Journal of Cataract & Refractive Surgery, 40(6), 870-887.

Plakitsi, A., O'Donnell, C., A Miranda, M., Charman, W. N., & Radhakrishnan, H. (2011). Corneal biomechanical properties measured with the Ocular Response Analyser in a myopic population. Ophthalmic and Physiological Optics, 31(4), 404-412.

Prata, T. S., Lima, V. C., Guedes, L. M., Biteli, L. G., Teixeira, S. H., de Moraes, C. G., Ritch, R., & Paranhos Jr, A. (2012). Association between corneal biomechanical properties and optic nerve head morphology in newly diagnosed glaucoma patients. Clinical & experimental ophthalmology, 40(7), 682-688.

Qi, J., He, W., Lu, Q., Zhang, K., Lu, Y., & Zhu, X. (2020). Schlemm canal and trabecular meshwork features in highly myopic eyes with early intraocular pressure elevation after cataract surgery. American Journal of Ophthalmology, 216, 193-200.

Quigley, H. A. (1987). Reappraisal of the mechanisms of glaucomatous optic nerve damage. Eye, 1(2), 318-322.

Quigley, H. A., Addicks, E. M., Green, W. R., & Maumenee, A. (1981). Optic nerve damage in

human glaucoma: II. The site of injury and susceptibility to damage. Archives of ophthalmology, 99(4), 635-649.

Quigley, H. A., & Broman, A. T. (2006). The number of people with glaucoma worldwide in 2010 and 2020. British Journal of Ophthalmology, 90(3), 262-267.

Quigley, H. A., Dunkelberger, G. R., & Green, W. R. (1989). Retinal ganglion cell atrophy correlated with automated perimetry in human eyes with glaucoma. American Journal of Ophthalmology, 107(5), 453-464.

Quigley, H. A., Hohman, R. M., Addicks, E. M., Massof, R. W., & Green, W. R. (1983). Morphologic changes in the lamina cribrosa correlated with neural loss in open-angle glaucoma. American Journal of Ophthalmology, 95(5), 673-691.

Quinn, G. E., Berlin, J. A., Young, T. L., Ziylan, S., & Stone, R. A. (1995). Association of intraocular pressure and myopia in children. Ophthalmology, 102(2), 180-185.

Rada, J. A. S., Shelton, S., & Norton, T. T. (2006). The sclera and myopia. Experimental eye research, 82(2), 185-200.

Rao, H. L., Addepalli, U. K., Jonnadula, G. B., Kumbar, T., Senthil, S., & Garudadri, C. S. (2013). Relationship between intraocular pressure and rate of visual field progression in treated glaucoma. Journal of glaucoma, 22(9), 719-724.

Read, S. A., Collins, M. J., & Sander, B. P. (2010). Human optical axial length and defocus. Investigative ophthalmology & visual science, 51(12), 6262-6269.

Rojananuangnit, K. (2021). Corneal Hysteresis in Thais and Variation of Corneal Hysteresis in Glaucoma. Clinical Optometry, 13, 287.

Rose, K. A., Morgan, I. G., Ip, J., Kifley, A., Huynh, S., Smith, W., & Mitchell, P. (2008). Outdoor activity reduces the prevalence of myopia in children. Ophthalmology, 115(8), 1279-1285.

Rudnicka, A. R., Kapetanakis, V. V., Wathern, A. K., Logan, N. S., Gilmartin, B., Whincup, P. H., Cook, D. G., & Owen, C. G. (2016). Global variations and time trends in the prevalence of childhood myopia, a systematic review and quantitative meta-analysis: implications for aetiology and early prevention. British journal of ophthalmology, 100(7), 882-890.

Ruiz-Medrano, J., Montero, J. A., Flores-Moreno, I., Arias, L., García-Layana, A., & Ruiz-Moreno, J. M. (2019). Myopic maculopathy: current status and proposal for a new classification and grading system (ATN). Progress in retinal and eye research, 69, 80-115.

Sankaridurg, P., Tahhan, N., Kandel, H., Naduvilath, T., Zou, H., Frick, K. D., Marmamula, S., Friedman, D. S., Lamoureux, E., & Keeffe, J. (2021). IMI Impact of myopia. Investigative ophthalmology & visual science, 62(5), 2-2.

Saw, S.-M., Katz, J., Schein, O. D., Chew, S.-J., & Chan, T.-K. (1996). Epidemiology of myopia. Epidemiologic reviews, 18(2), 175-187.

Saw, S.-M., Tong, L., Chua, W.-H., Chia, K.-S., Koh, D., Tan, D. T., & Katz, J. (2005). Incidence and progression of myopia in Singaporean school children. Investigative Ophthalmology & Visual Science, 46(1), 51-57.

Sawaguchi, S., Yue, B. Y., Fukuchi, T., Iwata, K., & Kaiya, T. (1993). Age-related changes of sulfated proteoglycans in the human lamina cribrosa. Current eye research, 12(8), 685-692.

Sayin, D. T., Altan, C., Solmaz, B., & Basarir, B. (2021). Comparison of corneal biomechanical properties in primary open angle glaucoma, normal-tension glaucoma, and ocular hypertension.

Schweitzer, J. A., Ervin, M., & Berdahl, J. P. (2018). Assessment of corneal hysteresis measured by the ocular response analyzer as a screening tool in patients with glaucoma. Clinical ophthalmology (Auckland, NZ), 12, 1809.

Seo, J. H., Kim, T.-W., & Weinreb, R. N. (2014). Lamina cribrosa depth in healthy eyes. Investigative Ophthalmology & Visual Science, 55(3), 1241-1251.

Shah, S., Laiquzzaman, M., Cunliffe, I., & Mantry, S. (2006). The use of the Reichert ocular response analyser to establish the relationship between ocular hysteresis, corneal resistance factor and central corneal thickness in normal eyes. Contact Lens and Anterior Eye, 29(5), 257-262.

Shah, S., Laiquzzaman, M., Mantry, S., & Cunliffe, I. (2008). Ocular response analyser to assess hysteresis and corneal resistance factor in low tension, open angle glaucoma and ocular hypertension. Clinical & experimental ophthalmology, 36(6), 508-513.

Shen, M., Fan, F., Xue, A., Wang, J., Zhou, X., & Lu, F. (2008). Biomechanical properties of the cornea in high myopia. Vision Research, 48(21), 2167-2171.

Sigal, I. A., Grimm, J. L., Jan, N.-J., Reid, K., Minckler, D. S., & Brown, D. J. (2014). Eye-specific IOP-induced displacements and deformations of human lamina cribrosa. Investigative Ophthalmology & Visual Science, 55(1), 1-15.

Silver, F. H., Jaffe, M., & Shah, R. G. (2018). Structure and behavior of collagen fibers. In Handbook of properties of textile and technical fibres (pp. 345-365). Elsevier.

Sit, A. J. (2014). Intraocular pressure variations: causes and clinical significance. Canadian Journal of Ophthalmology, 49(6), 484-488.

Smith, T., Frick, K., Holden, B., Fricke, T., & Naidoo, K. (2009). Potential lost productivity resulting from the global burden of uncorrected refractive error. Bulletin of the World Health Organization, 87, 431-437.

Spoerl, E., Boehm, A. G., & Pillunat, L. E. (2005). The influence of various substances on the biomechanical behavior of lamina cribrosa and peripapillary sclera. Investigative Ophthalmology & Visual Science, 46(4), 1286-1290.

Tan, N. Y., Koh, V., Girard, M. J., & Cheng, C. Y. (2018). Imaging of the lamina cribrosa and its role in glaucoma: a review. Clinical & experimental ophthalmology, 46(2), 177-188.

Tang, S. M., Rong, S. S., Young, A. L., Tam, P. O., Pang, C. P., & Chen, L. J. (2014). PAX6 gene associated with high myopia: a meta-analysis. Optometry and vision science, 91(4), 419-429.

Thakku, S. G., Tham, Y.-C., Baskaran, M., Mari, J.-M., Strouthidis, N. G., Aung, T., Cheng, C.-Y., & Girard, M. J. (2015). A global shape index to characterize anterior lamina cribrosa morphology and its determinants in healthy Indian eyes. Investigative Ophthalmology & Visual Science, 56(6), 3604-3614.

Tham, Y.-C., Li, X., Wong, T. Y., Quigley, H. A., Aung, T., & Cheng, C.-Y. (2014). Global prevalence of glaucoma and projections of glaucoma burden through 2040: a systematic review and meta-analysis. Ophthalmology, 121(11), 2081-2090.

Tsikripis, P., Papaconstantinou, D., Koutsandrea, C., Apostolopoulos, M., & Georgalas, I. (2013).

The effect of prostaglandin analogs on the biomechanical properties and central thickness of the cornea of patients with open-angle glaucoma: a 3-year study on 108 eyes. Drug Design Development and Therapy, 7, 1149-1156.

Tun, T. A., Thakku, S. G., Png, O., Baskaran, M., Htoon, H. M., Sharma, S., Nongpiur, M. E., Cheng, C.-Y., Aung, T., & Strouthidis, N. G. (2016). Shape changes of the anterior lamina cribrosa in normal, ocular hypertensive, and glaucomatous eyes following acute intraocular pressure elevation. Investigative Ophthalmology & Visual Science, 57(11), 4869-4877.

Tun, T. A., Wang, X., Baskaran, M., Nongpiur, M. E., Tham, Y. C., Nguyen, D. Q., Strouthidis, N. G., Aung, T., Cheng, C.-Y., & Boote, C. (2021). Determinants of lamina cribrosa depth in healthy Asian eyes: the Singapore Epidemiology Eye Study. British journal of ophthalmology, 105(3), 367-373.

Van Newkirk, M. R. (1997). The Hong Kong vision study: a pilot assessment of visual impairment in adults. Transactions of the American Ophthalmological Society, 95, 715.

Vantomme, M., Pourjavan, S., & Detry-Morel, M. (2013). The range of the waveform score of the ocular response analyzer (ORA) in healthy. Bull Soc Belg Ophthalmol, 322, 91-97.

Verkicharla, P. K., Ohno-Matsui, K., & Saw, S. M. (2015). Current and predicted demographics of high myopia and an update of its associated pathological changes. Ophthalmic and Physiological Optics, 35(5), 465-475.

Vianna, J. R., Lanoe, V. R., Quach, J., Sharpe, G. P., Hutchison, D. M., Belliveau, A. C., Shuba, L. M., Nicolela, M. T., & Chauhan, B. C. (2017). Serial changes in lamina cribrosa depth and neuroretinal parameters in glaucoma: impact of choroidal thickness. Ophthalmology, 124(9), 1392-1402.

Voorhees, A., Jan, N.-J., & Sigal, I. (2017). Effects of collagen microstructure and material properties on the deformation of the neural tissues of the lamina cribrosa. Acta biomaterialia, 58, 278-290.

Wang, B., Nevins, J. E., Nadler, Z., Wollstein, G., Ishikawa, H., Bilonick, R. A., Kagemann, L., Sigal, I. A., Grulkowski, I., & Liu, J. J. (2013). In vivo lamina cribrosa micro-architecture in healthy and glaucomatous eyes as assessed by optical coherence tomography. Investigative Ophthalmology & Visual Science, 54(13), 8270-8274.

Wang, D., Chun, R. K. M., Liu, M., Lee, R. P. K., Sun, Y., Zhang, T., Lam, C., Liu, Q., & To, C. H. (2016). Optical defocus rapidly changes choroidal thickness in schoolchildren. PLoS One, 11(8), e0161535.

Wang, J., Li, Y., Musch, D. C., Wei, N., Qi, X., Ding, G., Li, X., Li, J., Song, L., & Zhang, Y. (2021). Progression of Myopia in School-Aged Children After COVID-19 Home Confinement. JAMA ophthalmology.

Wang, N. L., Friedman, D. S., Zhou, Q., Guo, L., Zhu, D., Peng, Y., Chang, D., Sun, L. P., & Liang, Y. B. (2011). A population-based assessment of 24-hour intraocular pressure among subjects with primary open-angle glaucoma: the handan eye study. Investigative Ophthalmology & Visual Science, 52(11), 7817-7821.

Winawer, J., Zhu, X., Choi, J., & Wallman, J. (2005). Ocular compensation for alternating myopic and hyperopic defocus. Vision research, 45(13), 1667-1677.

Wong, T. Y., Ferreira, A., Hughes, R., Carter, G., & Mitchell, P. (2014). Epidemiology and

disease burden of pathologic myopia and myopic choroidal neovascularization: an evidence-based systematic review. American Journal of Ophthalmology, 157(1), 9-25. e12.

Wong, T. Y., Klein, B. E., Klein, R., Tomany, S. C., & Lee, K. E. (2001). Refractive errors and incident cataracts: the Beaver Dam Eye Study. Investigative Ophthalmology & Visual Science, 42(7), 1449-1454.

Wong, Y.-L., & Saw, S.-M. (2016). Epidemiology of pathologic myopia in Asia and worldwide. The Asia-Pacific Journal of Ophthalmology, 5(6), 394-402.

Wong, Y. L., Zhu, X., Tham, Y. C., Yam, J. C., Zhang, K., Sabanayagam, C., Lanca, C., Zhang, X., Han, S. Y., & He, W. (2021). Prevalence and predictors of myopic macular degeneration among Asian adults: pooled analysis from the Asian Eye Epidemiology Consortium. British journal of ophthalmology, 105(8), 1140-1148.

Wright, C., Tawfik, M. A., Waisbourd, M., & Katz, L. J. (2016). Primary angle-closure glaucoma: an update. Acta ophthalmologica, 94(3), 217-225.

Wu, P.-C., Chen, C.-T., Chang, L.-C., Niu, Y.-Z., Chen, M.-L., Liao, L.-L., Rose, K., & Morgan, I. G. (2020). Increased time outdoors is followed by reversal of the long-term trend to reduced visual acuity in Taiwan primary school students. Ophthalmology, 127(11), 1462-1469.

Wu, P.-C., Chen, C.-T., Lin, K.-K., Sun, C.-C., Kuo, C.-N., Huang, H.-M., Poon, Y.-C., Yang, M.-L., Chen, C.-Y., & Huang, J.-C. (2018). Myopia prevention and outdoor light intensity in a school-based cluster randomized trial. Ophthalmology, 125(8), 1239-1250.

Wu, W., Dou, R., & Wang, Y. (2019). Comparison of corneal biomechanics between low and high myopic eyes—a meta-analysis. American Journal of Ophthalmology, 207, 419-425.

Xu, Y., Ye, Y., Chen, Z., Xu, J., Yang, Y., Fan, Y., Liu, P., Chong, I. T., Yu, K., & Lam, D. C. (2022). Corneal Stiffness and Modulus of Normal-Tension Glaucoma in Chinese: Normal-tension glaucoma, stiffer or softer? American Journal of Ophthalmology.

Yang, Y., Li, X., Yan, N., Cai, S., & Liu, X. (2009). Myopia: a collagen disease? Medical hypotheses, 73(4), 485-487.

Yu, L., Li, Z.-K., Gao, J.-R., Liu, J.-R., & Xu, C.-T. (2011). Epidemiology, genetics and treatments for myopia. International journal of ophthalmology, 4(6), 658.

Zhang, J., & Deng, G. (2020). Protective effects of increased outdoor time against myopia: a review. Journal of International Medical Research, 48(3), 0300060519893866.

Zhang, L., Beotra, M. R., Baskaran, M., Tun, T. A., Wang, X., Perera, S. A., Strouthidis, N. G., Aung, T., Boote, C., & Girard, M. J. (2020). In vivo measurements of Prelamina and Lamina Cribrosa biomechanical properties in humans. Investigative Ophthalmology & Visual Science, 61(3), 27-27.

Zhang, L., Beotra, M. R., Baskaran, M., Tun, T. A., Wang, X. F., Perera, S. A., Strouthidis, N. G., Aung, T., Boote, C., & Girard, M. J. A. (2020). In Vivo Measurements of Prelamina and Lamina Cribrosa Biomechanical Properties in Humans. Investigative Ophthalmology & Visual Science, 61(3).

Zhou, X., Pardue, M. T., Iuvone, P. M., & Qu, J. (2017). Dopamine signaling and myopia development: what are the key challenges. Progress in retinal and eye research, 61, 60-71.

Zou, M., Wang, S., Chen, A., Liu, Z., Young, C. A., Zhang, Y., Jin, G., & Zheng, D. (2020). Prevalence of myopic macular degeneration worldwide: a systematic review and meta-analysis. British journal of ophthalmology, 104(12), 1748-1754.